

AFRL-IF-RS-TR-2002-320
Final Technical Report
January 2003



SONICFLIP: AN INTEGRATED PLATFORM FOR BIOFLUID MONITORING

University of Wisconsin

Sponsored by
Defense Advanced Research Projects Agency
DARPA Order No. E117


APPROVED FOR PUBLIC RELEASE; DISTRIBUTION UNLIMITED.

The views and conclusions contained in this document are those of the authors and should not be interpreted as necessarily representing the official policies, either expressed or implied, of the Defense Advanced Research Projects Agency or the U.S. Government.

AIR FORCE RESEARCH LABORATORY
INFORMATION DIRECTORATE
ROME RESEARCH SITE
ROME, NEW YORK

This report has been reviewed by the Air Force Research Laboratory, Information Directorate, Public Affairs Office (IFOIPA) and is releasable to the National Technical Information Service (NTIS). At NTIS it will be releasable to the general public, including foreign nations.

AFRL-IF-RS-TR-2002-320 has been reviewed and is approved for publication.

A handwritten signature in black ink, appearing to read "Tom Renz", with a large, sweeping flourish at the end.

APPROVED:

THOMAS E. RENZ
Project Engineer

A handwritten signature in black ink, appearing to read "Michael L. Talbert", with a large, sweeping flourish at the end.

FOR THE DIRECTOR:

MICHAEL L. TALBERT, Maj., USAF
Technical Advisor, Information Technology Division
Information Directorate

REPORT DOCUMENTATION PAGE			Form Approved OMB No. 074-0188	
Public reporting burden for this collection of information is estimated to average 1 hour per response, including the time for reviewing instructions, searching existing data sources, gathering and maintaining the data needed, and completing and reviewing this collection of information. Send comments regarding this burden estimate or any other aspect of this collection of information, including suggestions for reducing this burden to Washington Headquarters Services, Directorate for Information Operations and Reports, 1215 Jefferson Davis Highway, Suite 1204, Arlington, VA 22202-4302, and to the Office of Management and Budget, Paperwork Reduction Project (0704-0188), Washington, DC 20503				
1. AGENCY USE ONLY (Leave blank)		2. REPORT DATE JANUARY 2003		3. REPORT TYPE AND DATES COVERED Final Jun 00 – Jul 02
4. TITLE AND SUBTITLE SONICFLIP: AN INTEGRATED PLATFORM FOR BIOFLUID MONITORING			5. FUNDING NUMBERS C - F30602-00-2-0572 PE - 63739E PR - E117 TA - 00 WU - 59	
6. AUTHOR(S) Amit Lal				
7. PERFORMING ORGANIZATION NAME(S) AND ADDRESS(ES) University of Wisconsin Board of Regents Research Sponsored Programs 750 University Avenue Madison Wisconsin 53705-1490			8. PERFORMING ORGANIZATION REPORT NUMBER	
9. SPONSORING / MONITORING AGENCY NAME(S) AND ADDRESS(ES) Defense Advanced Research Projects Agency AFRL/IFTC 3701 North Fairfax Drive 26 Electronic Parkway Arlington Virginia 22203-1714 Rome New York 13441-4514			10. SPONSORING / MONITORING AGENCY REPORT NUMBER AFRL-IF-RS-TR-2002-320	
11. SUPPLEMENTARY NOTES AFRL Project Engineer: Thomas E. Renz/IFTC/(315) 330-3423/ Thomas.Renz@rl.af.mil				
12a. DISTRIBUTION / AVAILABILITY STATEMENT APPROVED FOR PUBLIC RELEASE; DISTRIBUTION UNLIMITED.				12b. DISTRIBUTION CODE
13. ABSTRACT (Maximum 200 Words) The work concerns the focused goal of developing technologies to miniaturize microfluidics for wrist-watch scale assays of biofluids such as interstitial fluids and blood. The platform consists of a microfluidic system driven by an array of piezoelectric pillars. This array is then driven by CMOS electronics. This architecture enables the division of manufacturing between IC manufacturers, piezoelectric chip producers, and microfluidic chip producers in a stacked manner that can fit in a wristwatch format. We demonstrate use of projected ultrasonic fields for distributed forces inside microchannels for programmable microfluidics inside plastic and silicon microfluidic structures. The work also demonstrates resonating structures inside microfluidic channels that can manipulate ultrasonic forces around the structures in a controlled manner for particle trapping. We also demonstrate a strategy for sub-5V and sub 5-milliWatt valve using piezoelectric unimorphs connected to the microfluidic chip via magnetically extruded pillars.				
14. SUBJECT TERMS Microfluidics, Biofluids, Piezoelectric Pillars, Wristwatch Format, CMOS Electronics, Sub-5-MilliWatt Valve				15. NUMBER OF PAGES 45
				16. PRICE CODE
17. SECURITY CLASSIFICATION OF REPORT UNCLASSIFIED	18. SECURITY CLASSIFICATION OF THIS PAGE UNCLASSIFIED	19. SECURITY CLASSIFICATION OF ABSTRACT UNCLASSIFIED	20. LIMITATION OF ABSTRACT UL	

Table of Contents

Section A: Summary & Introduction	1
Section B: PZT Array for Programmable Microfluidic Actuation	3
Project goals:.....	3
Documents available:.....	3
Results:.....	3
Future Efforts	4
Section C Circuits for Piezoelectric Array Drive	8
Goal:.....	8
Documents available:.....	8
Implementation:	8
Results:.....	8
Future Work:.....	8
Section D: Microstructure Resonant Drive for Microfluidic Actuator for Fluid Mixing	10
Goal:.....	10
Documents available:.....	10
Key Results:	10
Section E Embedded Beam Flow Sensor Integrated in Microfluidic Channel.....	13
Goal:.....	13
Documents available:.....	13
Results:.....	13
Analytical Model:	13
Experimental verification of principle using plastic devices:.....	13
Design of peizoresistors using simulation results – mask design:.....	15
Current Issues / Future work.....	17
Section F: Piezoelectric Microvavle	18
Goal:.....	18
Results:.....	18
Section G: Elastic Feedback System for Needle Insertion and Fluid Sampling.....	21
Goals of project:.....	21
Documents available:.....	21
Results:.....	21
Projected efforts and anticipated results with quantitative measures if possible:.....	22
Description of needle stage and components as shown in Figure G.2.....	23
Section H: Ultrasonic Separations and Pumping in Glass Capillary System	24
Documents available:.....	24
Results:.....	24
Section I: Broqnian-motion Simulation of Particles in the Presence of Acoustic Radiation	29
Goals of project:.....	29
Previous results and status from last PI meeting:	30
New results:	31
Next six month projected efforts and anticipated results with quantitative measures if possible:	32

Section J: Sensing protein conformational changes with resonant antennas	33
Goals:	33
Results:	33
New results:	34
Next six month projected efforts and anticipated results with quantitative measures if possible:	35
Appendix 1 List of Publications	37
Appendix 2 PATENTS: Disclosures/Filings with WARF (Wisconsin Alumni Research Foundation)	38
Appendix 2 Student Contributions	39

List of Figures

Figure A.1 Microfluidic System	2
Figure B.1 PZT Fluidic System	5
Figure B.2 PZT Pixels	6
Figure B.3 Photo of PZT System	7
Figure C.1 FPGA Circuit Board	9
Figure C.2 Sine, Cosine, and -Sine generation at 1 MHz	9
Figure D.1 Fluid Actuator	10
Figure D.2 PZT Plate Side View	11
Figure D.3 PZT Plate Side View With Cap	12
Figure E.1 Flow Sensor	13
Figure E.2 Model For In-channel Beam Bending Due to Flow	14
Figure E.3 Channel structure for testing	14
Figure E.4 Models vs. Experimental Results	14
Figure E.5 Piezoresistor Layout	15
Figure F.1 Piezoelectric Microvalve	18
Figure F.2 Magnetic Pillar Formation	19
Figure F.3 PZT/Nickel Unimorphs	20
Figure F.4 Unimorph Displacement	20
Figure G.1 Vertical Insertion of Micro-needle Array	21
Figure G.2 Needle Stage	22
Figure G.3 Needle Insertion and Pumping System	23
Figure H.1 A Typical Electro-osmotic Micro-fluidic Assay System	24
Figure H.2 Capillary Bending Mode	25
Figure H.3 Glass Capillary/PZT Transducer	26
Figure H.4 Capillary/PZT Transducer With Electrodes	26
Figure H.5 Two Half-wavelength Vibration Modes of the PZT Plate	27
Figure H.6 Impedance of the PZT/Glass Transducer	27
Figure H.7 Bead Separation at a Broad Antinode	28
Figure I.1 Intranode Separation	30
Figure I.2 Acoustic Filter	30
Figure I.3 1.25 Micron Particle Mixing	31
Figure I.4 1.5 Micron Particle Mixing	31

Figure I.5	Mixing Fraction Diagram	31
Figure I.6	Acoustic Chromatography	32
Figure J.1	Frequency Response of Air and RNase A	33
Figure J.2	Frequency Response of Air and RNase A at Various Temperatures	33
Figure J.3	Fitting of Representative Peaks	34
Figure J.4	Variation of Peak Position with Concentration of RNase A	34
Figure J.5	Variation of Peak 3 with RNase A Concentration	34
Figure J.6	Frequency Response of RNase A at Selected Temperatures	35
Figure J.7	Variation of Position of peak 5 with Temperature	35
Figure J.8	Fits of Data From Microwave and UV/VIS Measurements	35
Figure J.9	Results of Fitting of Data From Microwave and UV/VIS Measurements	35

Section A:

Summary & Introduction

The overall goal of the SonicFlip project is to create technologies that enable microfluidic integration at a wristwatch scale. Our basic guideline was that all actuation and sensing should be done with CMOS electronics compatible voltages, currents, and therefore power. Our goal is to make a technology in which CMOS electronics actuated by one or two lithium batteries can enable complex microfluidic function. The architecture we are developing includes a CMOS chip that drives an array of piezoelectric actuators that are in-turn bonded to a silicon microfluidic chip (See diagrams on next page). By driving the array of piezoelectric actuators at different phases, we can generate time-averaged forces in the liquid in microchannels leading to pumping and mixing. Since each pixel is under electronic control, we can achieve programmable forces inside microfluidic channels. We have also developed the ability to laser machine piezoelectric substrates to create not just pixels but also piezoelectric bimorphs for other actuation of silicon nitride diaphragms. Another fabrication development has been the development of a method to create pillars of magnetic materials between the PZT and the silicon structure enabling automatic aligned bonding between the two substrates. The same technique to make pillars using magnetic extrusion is also being used to develop microneedle fabrication. In addition to above achievements, we have developed novel methods to acoustically separate polystyrene beads by different sizes in a optically observable aperture. This ability leads to perform multiple assays with different size beads, each coated with different antibodies. This capability adds to our capability to integrate assay capability in our microfluidic systems. Another area of achievements is that of using surface micromachine ultrasonic actuation from the external piezoelectric actuators. That line of work has led to vortex particle collector for sample concentration and unique pumping mechanisms. On the sensing front, a unique flow sensor paradigm based on drag on beams inside flow channel has been invented and implemented. By placing these beams onto Wheatstone bridges used as strain gauges, we can electronically detect the flow. This flow sensing method is scalable to nanoscale and approach flow sensing similar to beam sensors used by micro and millimeter scale biological cells and insects.

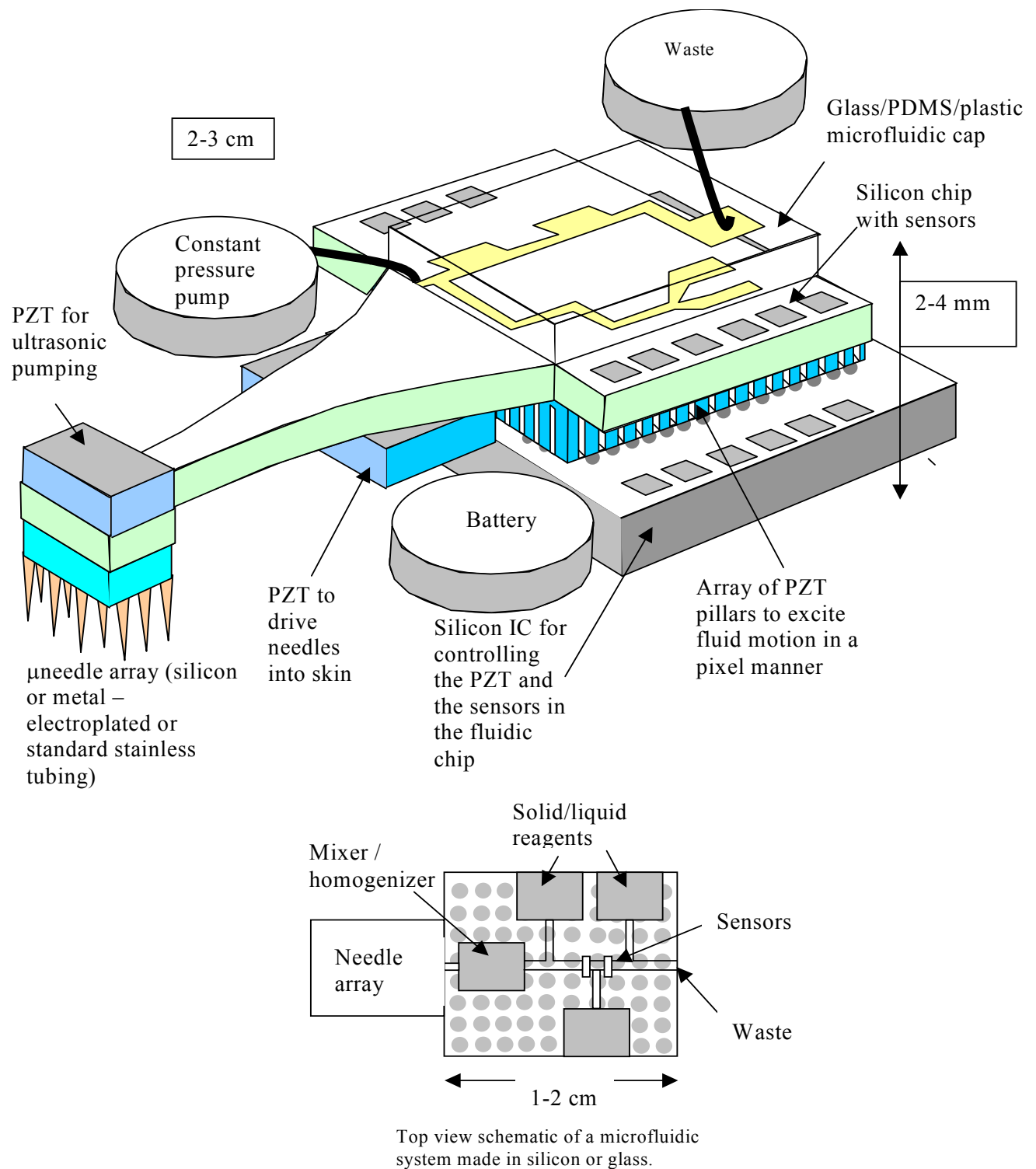


Figure A.1 The wristwatch size microfluidic system that samples interstitial fluid, inserts needles effortlessly (automatically), contains on-board pressurized liquid sources, battery, and a reconfigurable microfluidic system.

Section B:
PZT Array for Programmable Microfluidic Actuation
Jomar Ochoco (Masters student) and Amit Lal

Project goals:

For our Sonicflip system, a two dimensional microfluidic system is needed to actuate the body fluid through various channels where the contents of the fluid can be checked. We are accomplishing this task through the implementation of a two dimensional PZT pixel array. Each pixel in the array can be driven with different frequencies, amplitudes, and phases, which can result in programmable acoustic field gradients. One of the advantages of this approach is the fact that with acoustic streaming, disposable microfluidic cassettes of wide variety of materials that can be driven ultrasonically can be used as long as they can be interfaced to the piezoelectric array. Furthermore, since acoustic streaming is sensitive to only the viscosity of the liquid, a quantity that does not vary much for aqueous solutions, our system should be applicable to wide ranges of liquids, without regard to the conductivity and pH, as is the case in electrophoretic and electro-osmotic flow.

Documents available:

1. Ochoco, J., Lal, A., "Programmable Acoustic Streaming on a 2D PZT Pixel Array," IEEE Ultrasonics, Ferroelectrics, and Frequency Control Society Symposium, 2001, Atlanta
2. Ochoco, J., Lal, A., "Resonance Frequency Tuning of Two-Dimensional PZT array using Laser Trimming," IEEE Ultrasonics, Ferroelectrics, and Frequency Control Society Symposium, 2001, Atlanta
3. Masters Thesis for Jomar Ochoco on 2D Ultrasonic Microfluidics
4. Analytical derivation of acoustic field in 2D pixel array driven microfluidic system

Results:

Theory supporting the programmable acoustic forces has been developed as shown in the attached document concerning acoustic fields inside microfluidic channels. A series solution for the 3D acoustic field inside a channel with arbitrary surface acoustic velocities and top rigid boundary conditions has been developed. This theory will allow the calculation and optimization of the streaming forces in the near future after the fast calculations applied by implementation in the C programming language.

We developed a process for making PZT plates with grooves cut into them, that defines the individual pixels. A holder with pogo pins was designed, which made electrical contact, but still allowed for motion in the PZT. We chose to drive each pixel at the same resonant frequency and amplitude, but with variations in phase. This simplifies the circuitry because only two driving signals are needed: sine and cosine. Just changing the phase of one pixel can create many different acoustic field gradients. The circuitry implementing this strategy has been built. Frequency independent phase shifters were shown to work at frequencies between 3 and 14 MHz. The computer controlled crosspoint switch allows the user to determine the phase for each pixel. This system has allowed us to test fluid flow on top of the PZT pixel array.

Recent work has focused on characterization of the flow on top of the pixel array and determining the velocity based on variations in the signal amplitude. We were able to do this by observing the motion of 17 μm microspheres placed in the fluid. For a drive voltage of 1 Vpp, the particle velocity was 122 $\mu\text{m/s}$. A velocity of 1.65 mm/s is possible with only 3 Vpp. Furthermore, the velocity-amplitude follows an expected square relationship due to the acoustic streaming force dependence on the square of the acoustic velocity.

Work has also been done in the area of laser trimming of each pixel. Because of the small variations in resonant frequencies for the pixels in the area, a method is needed where all pixels can be tuned to the same resonant frequency. Removing material from a pixel will raise its resonant frequency and this can be done using a laser. We have shown that ten cuts with a 40 mW laser can increase the resonant frequency 15 kHz. Additionally, the impedance of the transducer decreases, indicating a lower loss resonator. At higher laser powers, depoling may occur, which can damage the PZT and increase its impedance.

Work is underway on PZT arrays of smaller dimensions with the major challenge being a substrate to bond the PZT to. We have solved this problem by fabricating circuit boards with small copper pads, which will contact each PZT pixel with a conductive paste. Pixels of 1mm and 0.5 mm will be looked at with the goal of making arrays with more elements and with smaller pixels.

Future Efforts

Future work will involve the smaller PZT pixels and possible schemes for connection to the controlling circuitry. Microfluidic channels in PDMS are also being tested, which can be placed on top of the PZT array. Challenges here include the acoustic coupling of the PDMS to the PZT. Characterization of the PZT pixel motions will also be investigated. An interferometer setup can be used to examine the motion on top of the array. Mathematical models will also be made that can simulate the acoustic fields being created by the pixels.

Digital sine wave generation has been developed and will be combined with the phase shifter circuitry for a standalone phase control system for the array.

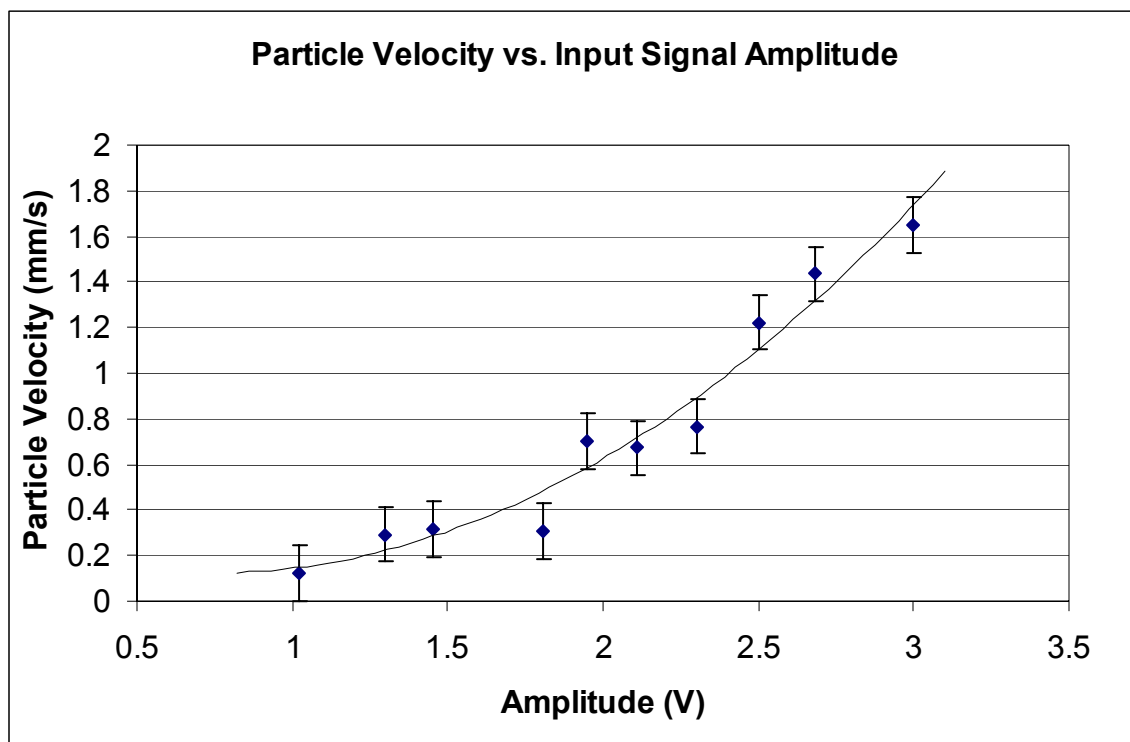
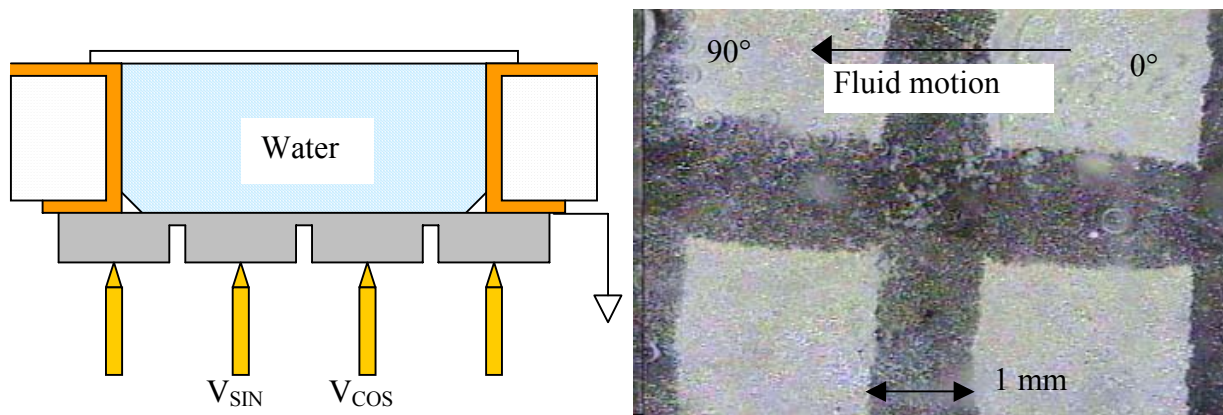


Figure B.1. Top left shows schematic of a PZT plate cut into pixels and electrodes with pogo pins. A water channel is formed by bonding a plastic cover with a gap layer. Right that flow changes direction from right to left as phase is changed by 90 degrees. Bottom shows the measured liquid velocity in the liquid bulk as a function of applied voltage on the pixels.

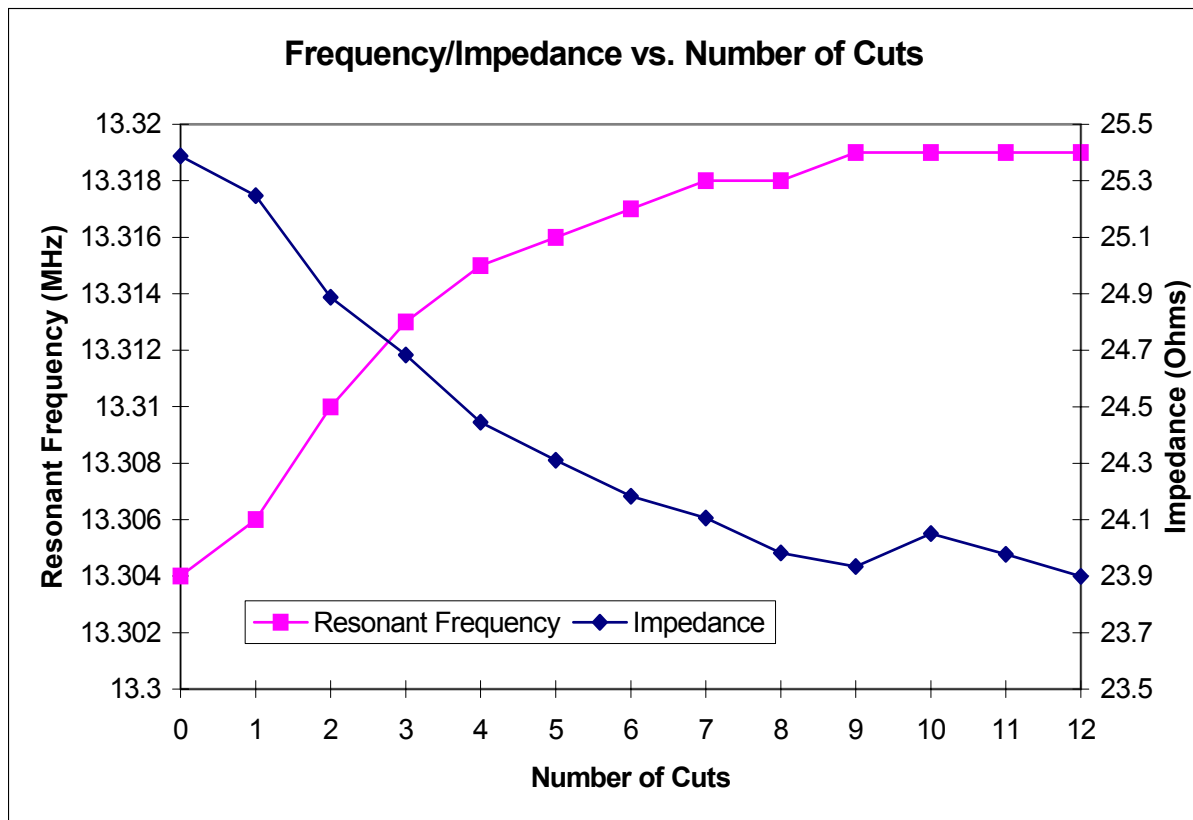
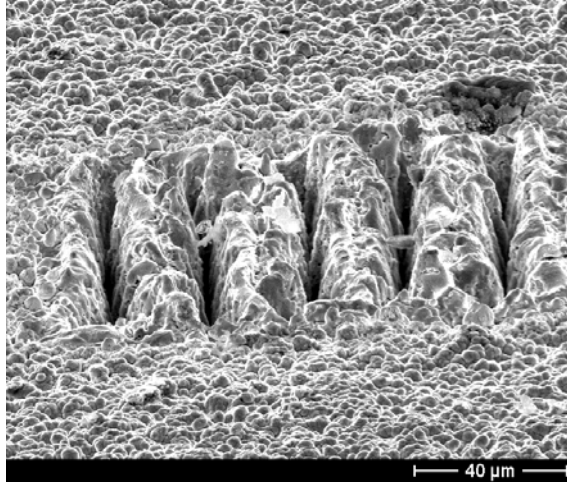


Figure B.2. Top shows SEM images of PZT pixels trimmed by laser melting and ablation of the nickel electrodes. Bottom shows the change in series resonance frequency and the equivalent series resistance of the pixel as a function of number of laser cuts on the PZT.

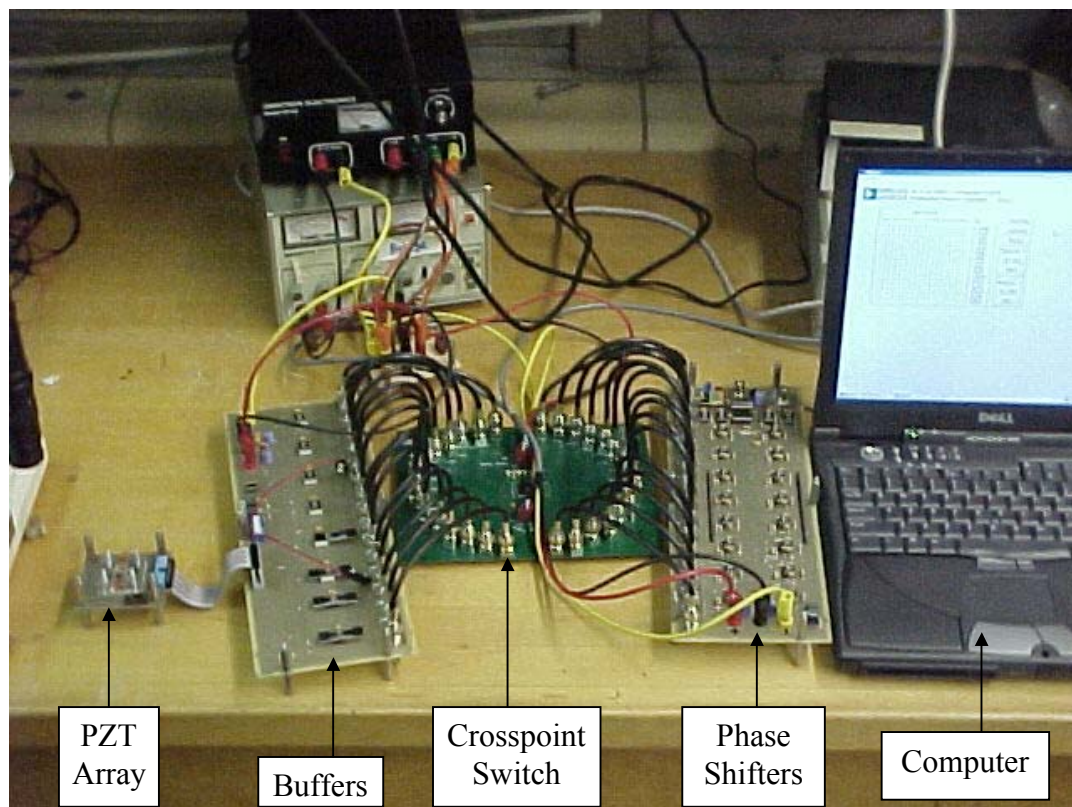


Figure B.3. A photograph of the computer controlled switching matrix, phase shifters, and the PZT array for microfluidics.

Section C

Circuits for Piezoelectric Array Drive

Jomar Ochoco (Masters student), Enny Kho (Undergraduate), and Amit Lal

Goal:

Due to the requirements of the phase shifter circuit for the PZT pixel array, a quadrature sinusoidal wave generator was needed. This device needs to create four sine waves with phases 0, 90, 180, and 270 degrees. In addition, the frequencies created need to cover a large bandwidth, from 100 kHz to 15 MHz, so that different resonant frequencies can be excited. The frequency should be changed in increments as small as 100 Hz.

Documents available:

1. Enny Kho's One-year report on Quadrature Generation

Implementation:

This goal has been nearly achieved using the Xilinx Spartan2 FPGA, which is programmed with XSA100 circuit board from XESS. Using the Direct Digital Synthesis (DDS) module from Xilinx, a sine and cosine wave generator was created. The DDS module creates the lookup tables and the counters that make this possible.

These digital outputs are connected to digital-to-analog converters from Analog Devices (AD7127). Because complementary outputs are created, the two digital FPGA outputs become four analog signals with two DACs.

Results:

The prototype creates four sinusoid waves with a maximum frequency above 2.5 MHz. Above that, there is more quantization error, which gives the wave the appearance of steps, rather than a pure curve. The minimum frequency is 800 Hz, which is also the frequency resolution. Power consumption was measured to be 2 W for the entire system.

Future Work:

By increasing the input clock frequency to the FPGA and optimizing the internal layout of our circuit in the FPGA, the maximum frequency can be increased. Another possible solution involves using the Virtex2 FPGA from Xilinx, which can handle higher clock frequencies. To improve the frequency resolution, more input bits can be added, but this can affect the maximum frequency. Optimized layout can also reduce these effects. Filters and amplifiers will be added to reduce noise and quantization error. Power consumption can be reduced as well, but must be done in such as to not lose speed. Lastly, we plan to add a microcontroller for control of the entire system. The microcontroller will control the FPGA inputs and process the FPGA outputs with a counter circuit and can then provide closed loop feedback control. An additional LCD display will give the user an interface for an easy to use standalone system. This can be used for any acoustic application requiring input signals with different phases.

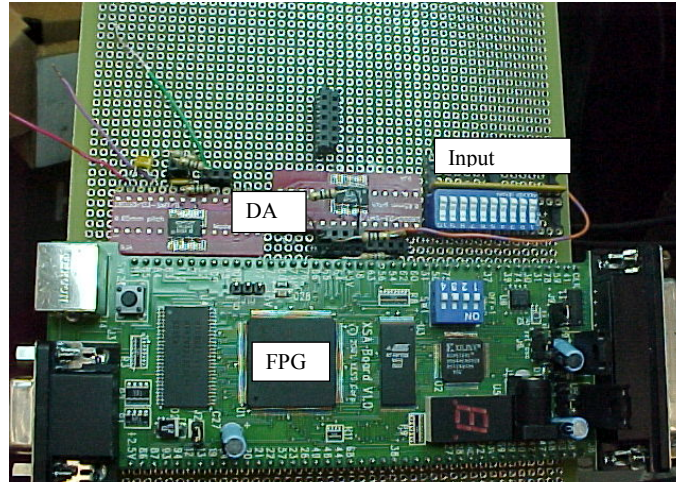
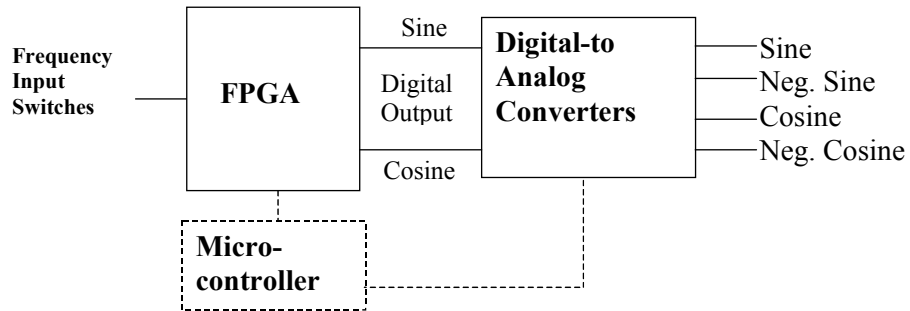


Figure C.1. The schematic and the PC board displaying the FPGA circuit board

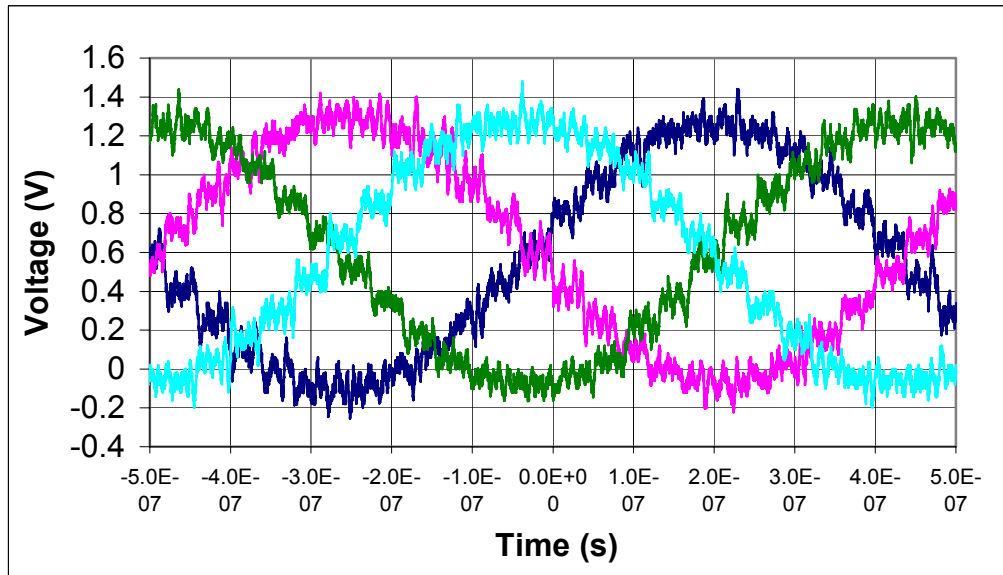


Figure C.2. Sine, Cosine, and -Sine generation at 1 MHz

Section D:
**Microstructure Resonant Drive for Microfluidic Actuator for Fluid
Mixing and Particle Capture**
Abhijit Sathaye (M.S. student), Ville Kajaakari (Ph.D. student) and Amit Lal

Goal: The goal of this research in general is to investigate the use of resonating microstructures inside microfluidic channels. The surface micromachines inside the channels are excited in their resonances by pixels of piezoelectric actuators.

Documents available:

1. Sathaye, A., Lal, A., "An acoustic vortex particle concentrator," Proceedings of the μ TAS 2001 Conference, Monterey, CA, pp. 185-187, Kluwer
 2. Sathaye, A., Lal, A., "An acoustic vortex generator for microfluidic particle entrapment," IEEE Ultrasonics, Ferroelectrics, and Frequency Control Society Symposium, 2001, Atlanta
 3. Kaajakari, V., Sathaye, A., Lal, A., "A Frequency Addressable Ultrasonic Microfluidic 4. Actuator Array," Digest of Technical Papers, International Conference on Solid State Sensors and Actuators, Munich, pp. 958-961
- Masters thesis for Abhijit Sathaye

Key Results:

- Developed a microfluidic actuation paradigm and achieved addressable fluid actuation over a wide frequency range (100kHz ~ 10Mhz).
- Fluid actuation obtained by a single PZT die at the back of Si sample, a structure that is simple and potentially inexpensive and consumes little power.
- Variety of fluidic effects observed in a fluidic channel of effective Reynold's number of 0.1
- A raw CFD simulation model for fluid flow around resonating microstructures inside a microfluidic channel developed (Work in progress).
- New devices with cornered actuator geometries (triangle, pentagon, hexagon) developed to ascertain / verify effect of actuator geometry on fluid vortex formation.
- To overcome the stiction problem of SU-8 during sample release, the new devices have more etch-holes reducing the release time down from ~20 minutes to less than 5 minutes.
- A process flow for a device with SU-8 walls and teflon-heat shrink cap (giving a variable height inside the channel) developed.

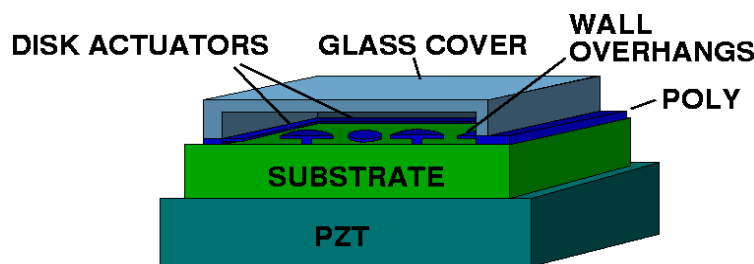


Figure D.1 Fluid Actuator

Next six month projected efforts and anticipated results with quantitative measures if possible:

- CFD simulation – Anticipated result : A model to predict the vortex formation for given flow rate, channel height and applied frequency. (April end)
- Work on the fluid samples to get more data on vortex formation. Experimental details : 1. Use of 2-section PZT to drive the two hubs with different signals and study the particle capture effect. (Refer fig. 1,2,3) 2. Use of real world samples, eg blood. (February end)

Develop a closed loop system : Particle localization by actuating the hub – a feedback signal from this to initiate next action eg, change actuation signal.(March end)

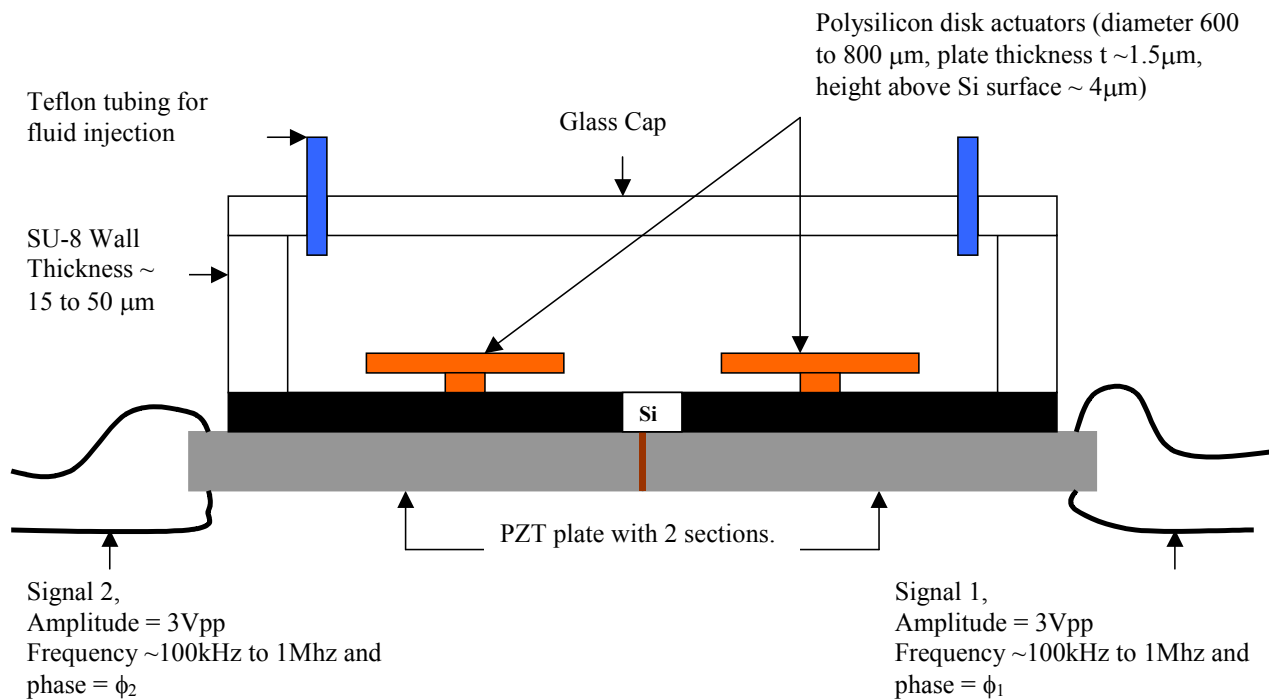


Figure D.2 Side view of structure in Figure D.1

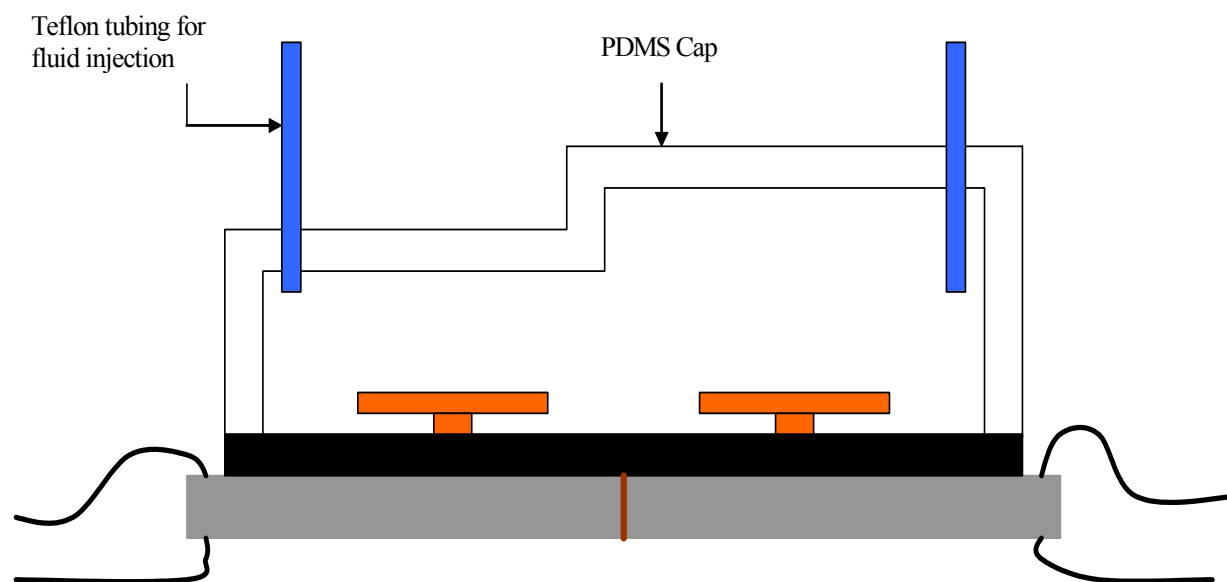


Figure D.3. Side view of structure in Figure D.1 with PDMS cap.

Section E

Embedded Beam Flow Sensor Integrated in Microfluidic Channel

Shankar Radhakrishnan (PhD student), Harun Solak (Postdoc), and Amit Lal

Goal: Enable flow sensing in the acoustically driven microfluidic system with electronic readout. The performance of the sensor in terms of power consumption, sensitivity, and repeatability is to be optimized.

Documents available:

Radhakrishnan, S., Solak, H., Lal, A., “In-channel flow sensor using drag forces,” Proceedings of the μ TAS 2001 Conference, Monterey, CA, pp. 179-181, Kluwer

Results:

Flow sensors are integrated inside the microfluidic channel to enable flow characterization using an array of flow sensors as well to provide feedback control of flow. For low Reynolds number flow ($Re \ll 1$), viscous forces dominate inertial forces. This flow sensor measures flow using the drag forces acting in a direction transverse to the direction of flow in the channel.

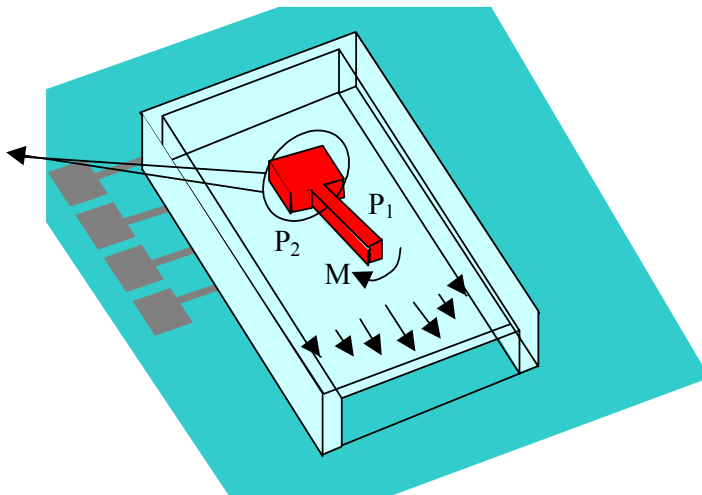


Figure E.1 Flow Sensor

The flow sensor consists of a cantilever beam, anchored at the upstream end, placed at a small angle to the direction of flow as shown in figure 1.

The beam divides the channel into n equal parts (1 & 2) causing different flow profiles in the two parts. This causes two different pressure gradients (P_1 & P_2) on the two sides of the beam, causing a net force, transverse to the direction of flow. This force may cause a deflection of the beam for a flexible beam or cause a net moment 'M' translated to the anchor in the case of rigid beams. Flow can be sensed by measuring either the tip displacement of

the beam or the stress in the anchor using a piezoresistive bridge network as described later.

Analytical Model: We developed an analytical model for the flow sensor. The model is summarized in Figure E.2

Experimental verification of principle using plastic devices: We demonstrated proof of concept using plastic devices (SLA fabricated at Becton Dickinson). Figure E.3 shows a plastic device with input and output fluidic ports.

2D and 3D models for flow around microbeams were developed using a code CFDRC.

Simulated values matched experimental results from the plastic devices. The results are shown in Figure E.4.

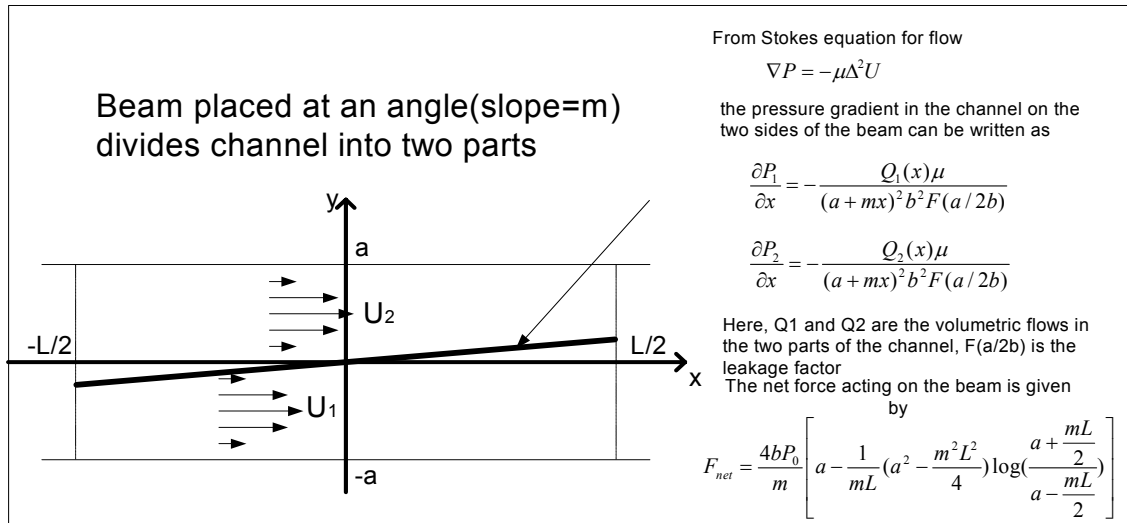


Figure E.2 Model for in-channel beam bending due to flow.



Figure E.3 Channel structure for testing

SLA fabricated device

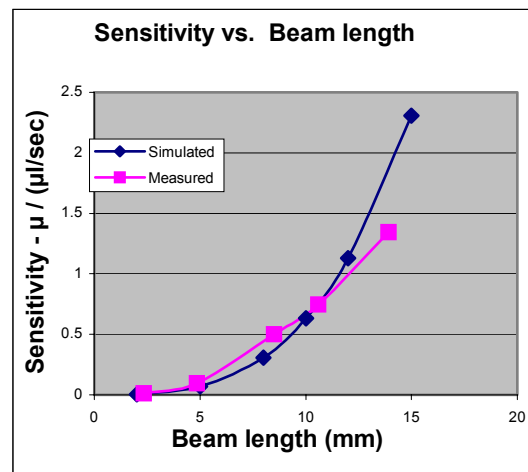
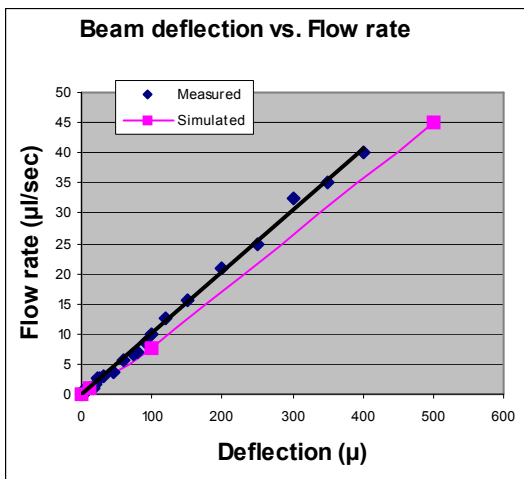


Figure E.4 Models vs. Experimental Results.

Design of piezoresistors using simulation results – mask design: Using simulations, we obtained the stress distribution underneath the anchor. These results were used to design piezoresistive layout underneath the anchor to sense the flow. An example of a layout is shown in the SEM in Figure E.5.

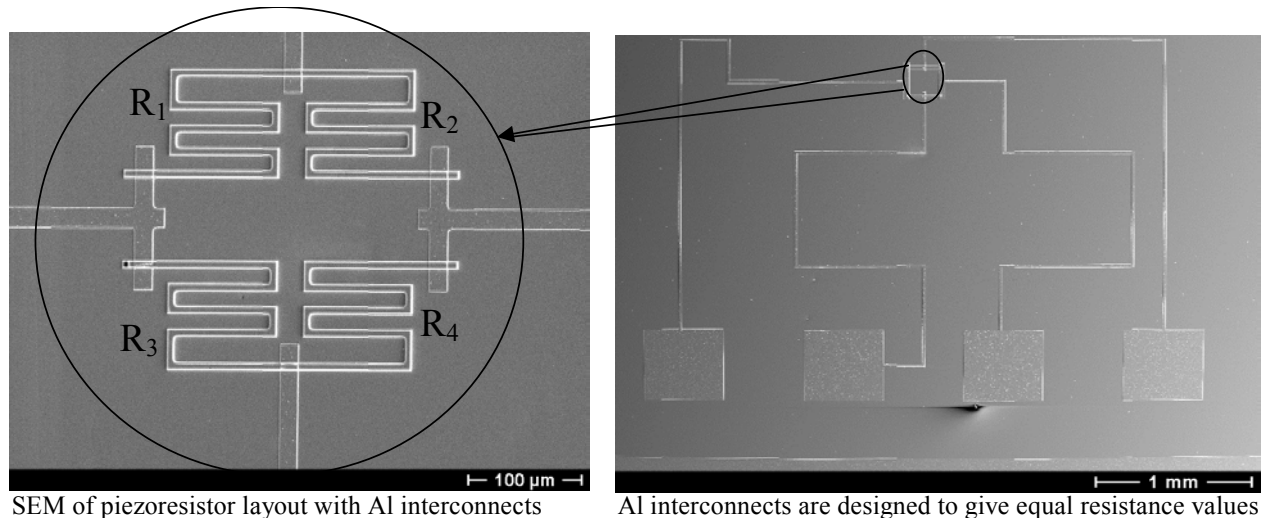
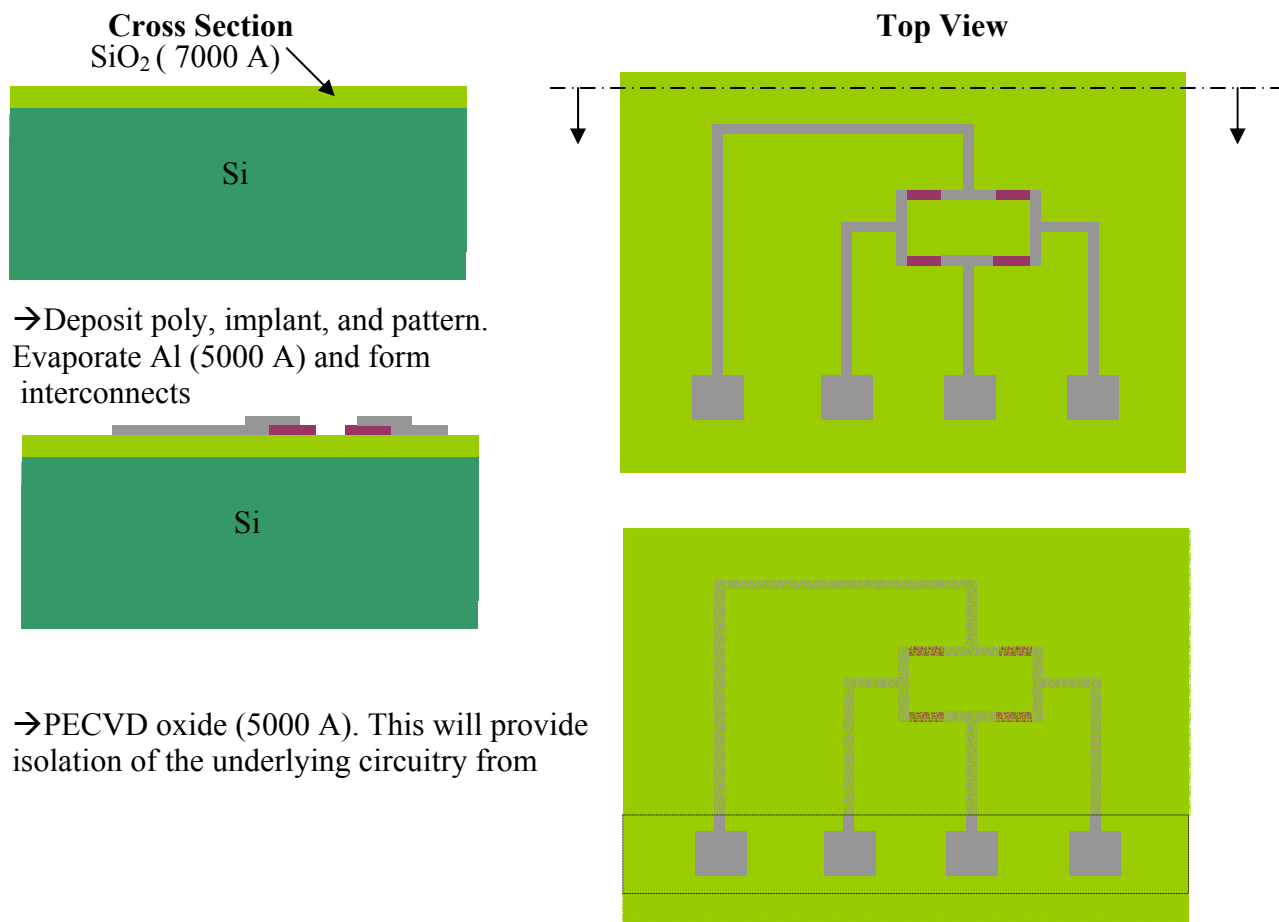


Figure E.5 Piezoresistor Layout.

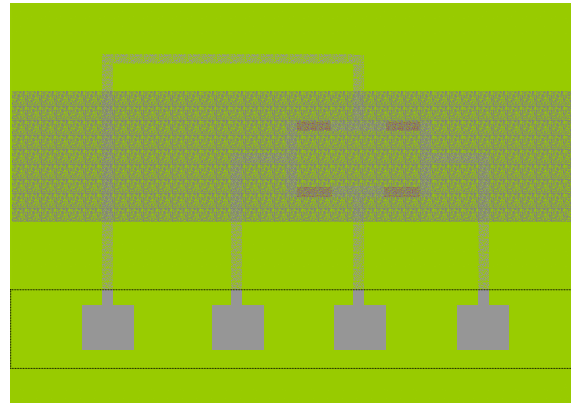
We are developing a process flow to fabricate the structure with Nickel cantilever. The six mask process flow is described below.



the channel.



→ Top view (right) shows dotted regions corresponding the area in which PECVD oxide is etched away to access the Al contact pads

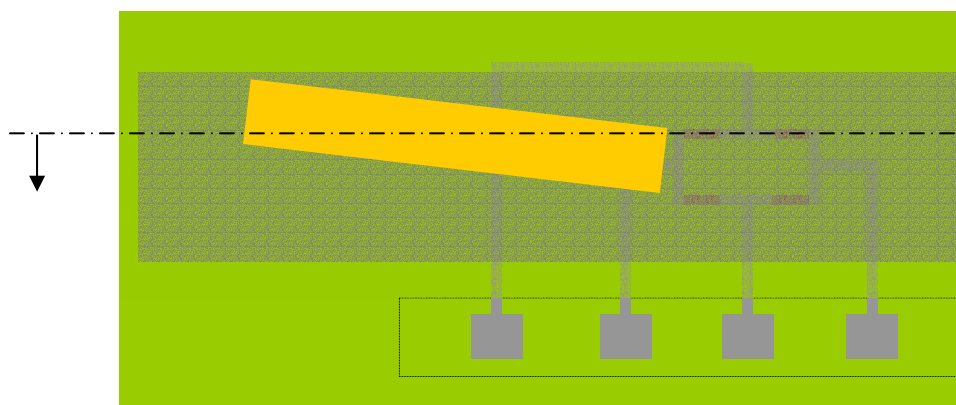


→ A seed layer of Cr/Cu/Cr for Ni electroplating is formed using a liftoff step.

→ A 3000 Å thick gold layer is formed as a sacrificial layer to release the Ni cantilever

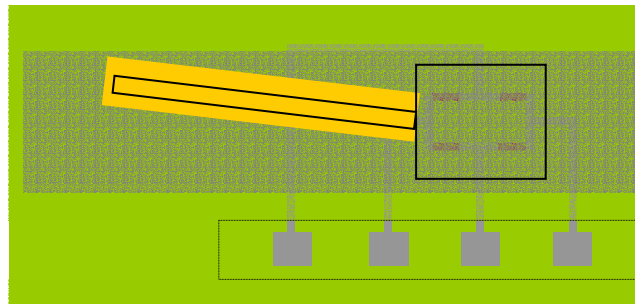


Cross Section



Top view

→ A mold is then patterned over the seed layer such that the cantilever part of the mold lies over the gold sacrificial layer.



→ Nickel electroplating to form the cantilevers.



→ Cantilevers are released by etching the sacrificial gold layer.



Current Issues / Future work

- Resist thickness – Currently, we are using molds of thickness up to 20 microns to electroplate Nickel. We can increase this by multiple coats of the resist.
- While using gold etchant to release the cantilevers, chromium (which is part of the seed layer) is attacked vigorously. We will investigate other metals or photoresists for sacrificial in future.
- To demonstrate closed loop control of flow using the output of the piezoresistive network.

Section F: Piezoelectric Microvalve

Rajesh Duggirala (MS student), Il-Seok Son (PhD student), and Amit Lal

Goal: Following the philosophy of controlling all microfluidic components by sub-5V signals, we need to also be driven at low voltages. We chose to investigate the possibility of using piezoelectric unimorphs fabricated by laser cutting into PZT plates, which will also contain the PZT pixels for flow control. Hence the PZT chip now serves also to actuate valves.

Results:

The development of the valves is ongoing, but progress has been made in the following areas:

1. Development of piezoelectric unimorphs made by laser cutting PZT plates. A 355 nm laser has been setup previously for PZT trimming. However, at high power it has been found to be useful to cut PZT ceramics reproducibly with 100 micron features on a 500 micron thick plate.
2. Development of a pillar formation process to connect the PZT unimorphs at one level to silicon nitride membranes in the silicon chip connected to the PZT chip. For this purpose we developed a magnetic extrusion process by which magnetically active epoxy is lifted by a magnet to the silicon nitride wafer. This process allows the elimination of accurate placement on the silicon chip over the PZT chip. This is shown in the Figure below.
3. Measurement of membrane displacement – approximately 3 micron displacement at 5 V drive at the bimorph is possible at dc. Resonant drive at 2 and 3 kHz results in substantially more displacement. Hence, resonant drive could be used to pump as well seal off liquid.
4. Valve function: Currently the flow sensor and the valve are being integrated on one chip to demonstrate electronic control of flow. We hope to demonstrate closed loop control by August 23.

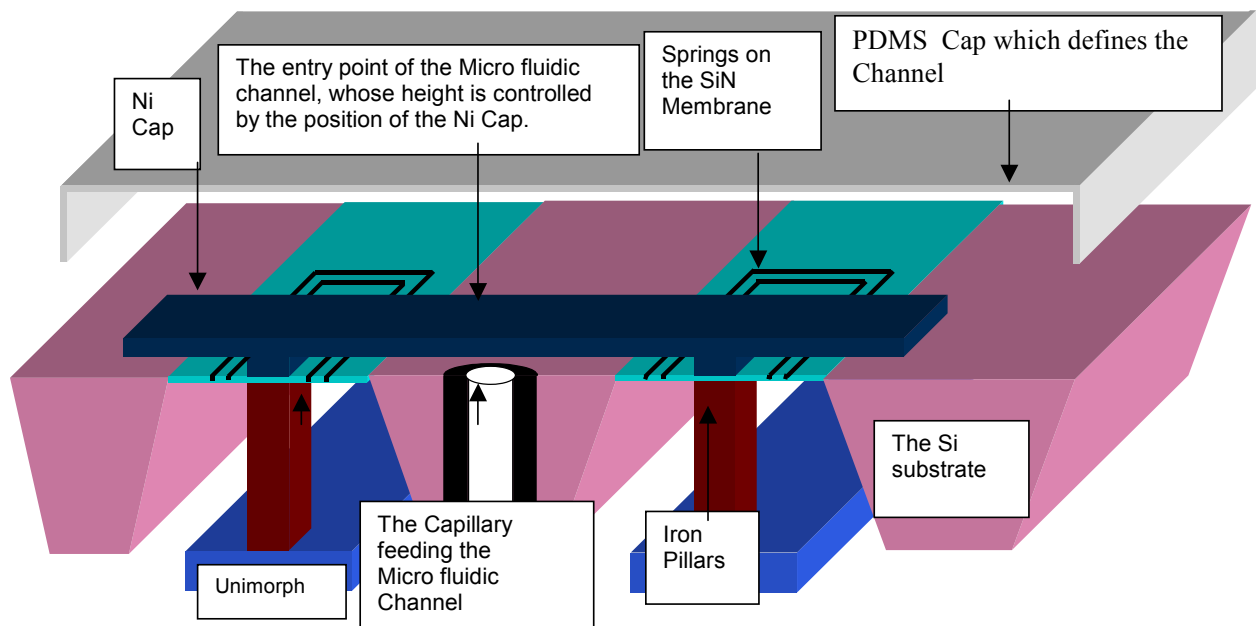


Figure F.1 Piezoelectric Microvalve.

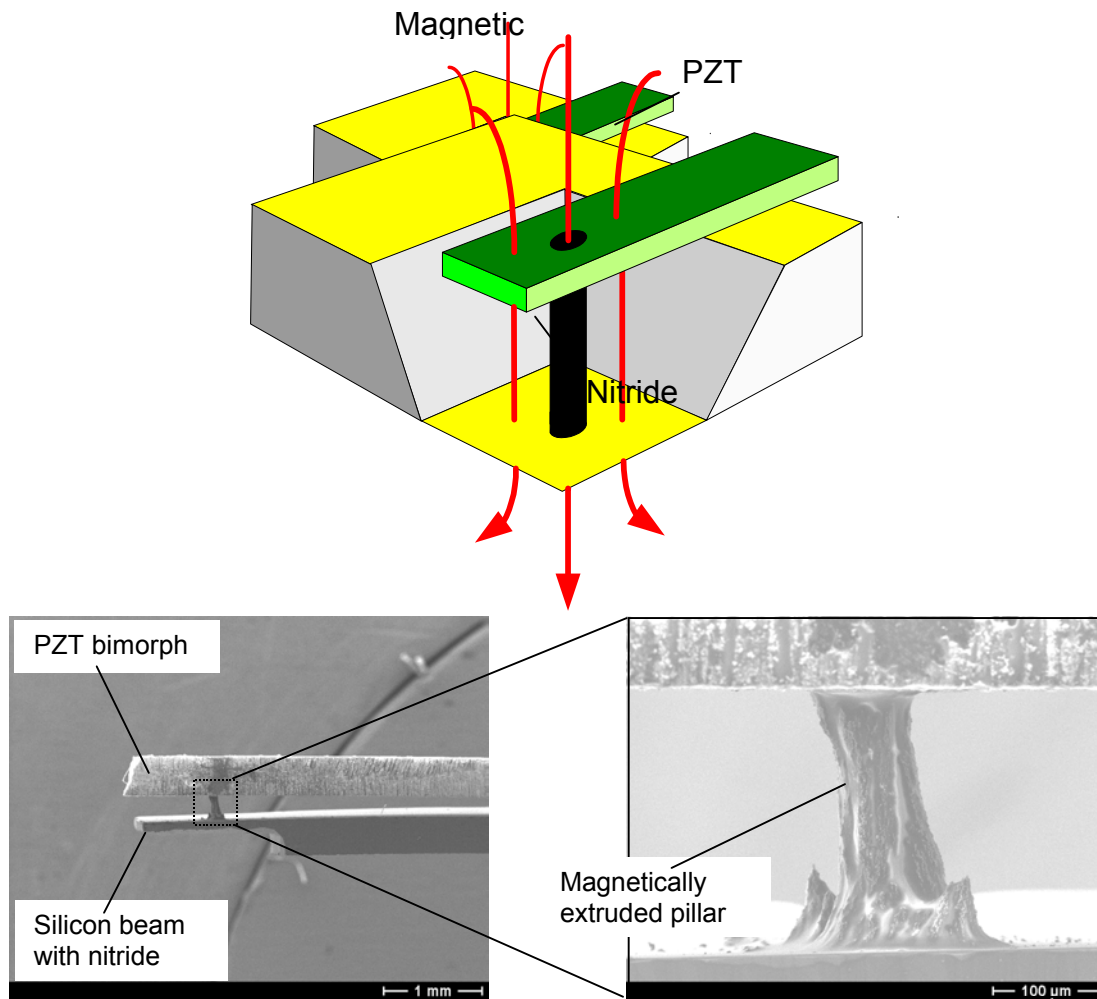


Figure F.2. Top shows the schematic to pull up a magnetic pillar. Left shows the forming of a pillar between a PZT bimorph and a silicon beam. Right shows close-up of the pillar. Note that even though the pillar shape is not clean, the self-alignment feature from the unimorphs to silicon allows proper coupling.

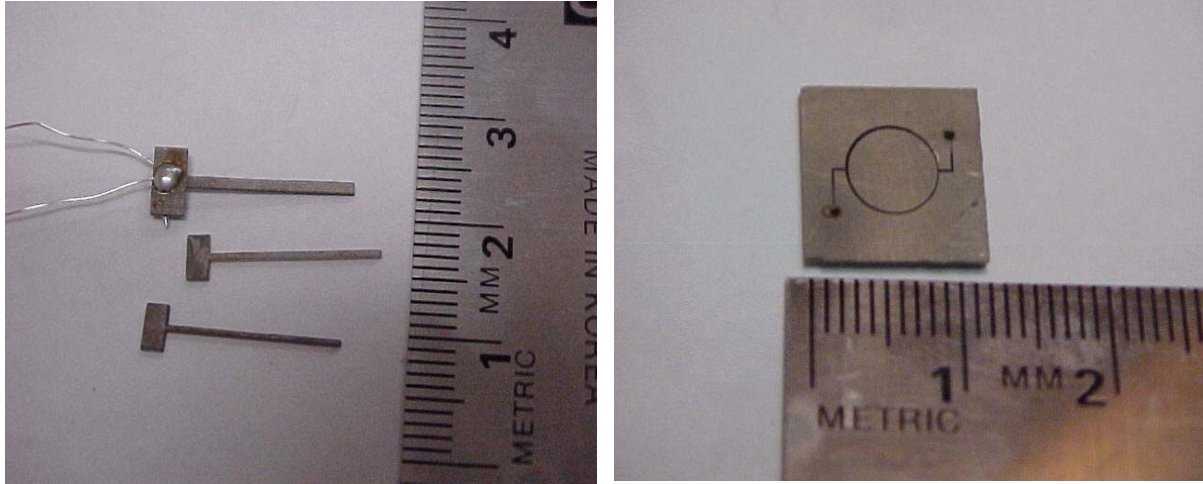


Figure F.3. Left shows PZT/Nickel unimorphs laser cut out of PZT plates. Right shows channels laser cut into a PZT plate.

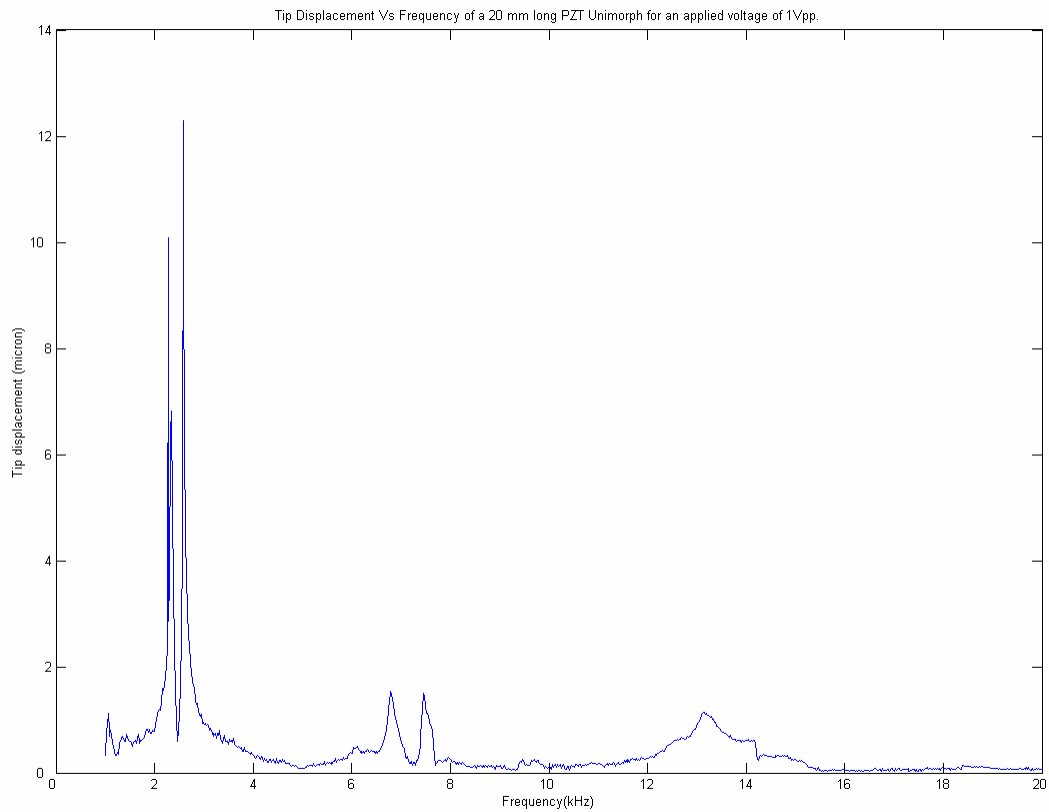


Figure F.4. The unimorph displacement versus applied voltage of 1 Vpp for a 20 mm by 2 mm long unimorph.

Section G:

Elastic Feedback System for Needle Insertion and Fluid Sampling

Xi Chen (Ph.D. student) and Amit Lal

Goals of project:

Develop microneedle structures for BioFlip platform. Also provide a stage for mounting hypodermic needles for skin penetration and incorporation of ultrasonic capillary pump for ISF/blood sampling.

Documents available:

1. Chen, X., Lal, A., "Integrated Pressure and Flow Sensor in Silicon-Based Ultrasonic Surgical Actuator," IEEE Ultrasonics, Ferroelectrics, and Frequency Control Society Symposium, 2001, Atlanta
2. Chen, Xi, Lal, A., "Micromachined Ultrasonic Ophthalmic Microsurgical tool with integrated Pressure sensor," Digest of Technical Papers, International Conference on Solid State Sensors and Actuators, Munich, pp. 424-427

Results:

A vertical insertion stage has been designed for inserting fixed amount of micro needle into skin (Figure G.1). The needle array is to be mounted on the tip of a silicon needle and the force against skin is applied by driving the silicon needle in bimorph mode. This design possesses a few difficulties. First, the fabrication and assembling of micro needle arrays are complex and though skin penetration by micro needle arrays is a topic of active research now, it is far from a mature technology and would require extra time for the accomplishment of the whole project. Second, incorporation of pumping and fluid transport mechanisms that are currently evaluated by other subprojects is difficult. Based on this situation and the results from related subprojects a new parallel insertion stage with elastic feed back is designed since last PI meeting.

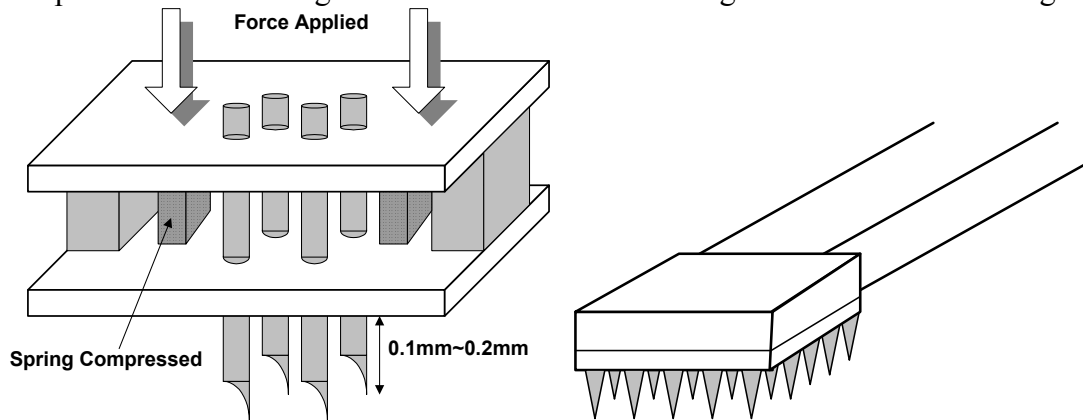


Figure G.1: vertical insertion of micro-needle array

The elastic feedback needle stage is shown in Figure G.2. This prototype stage is made in wood and elastic rubber bands. The rubber bands provides elastic feedback and adjustment on the force applied on the needle as it proceeds against the skin, resembling the adjustment in hand operated needle insertion: increased force when the skin resists the needle and decreased force when the skin is penetrated by the needle. Conventional stainless steel hypodermic needle can be used in

this design. Glass capillary is aligned with the needle and is driven ultrasonically with attached piezoelectric PZT plate to pump fluid. Some results and discussions of this device are listed below.

1. The stage with needle and pump can be bonded on forearm or other convenient place to perform insertion and sampling.
2. Ultrasonic glass capillary pump was studied by Chunghoon Lee and Amit Lal. Here the emphasis is on incorporation of hypodermic needle and capillary pump. The combination of the two as shown in Figure 2 has been tested to pump water successfully.
3. Ultrasonic capillary pump works by atomization and acoustic streaming. Both pumping of water accompanied by strong atomization at the opening of the capillary and pumping realized through continuous up flow of water are observed. However, since the lower part of the capillary is confined inside the needle and its mechanical conditions there vary easily, the atomization mechanism is more reliable and repeatable.
4. The pumping works most effectively at $\sim 450\text{kHz}$ with 10V_{pp} driving voltage. The exact working frequency may vary slightly from run to run or during continuous pumping.
5. Capillary effect is essential for the fluid to fill up the glass capillary before atomization at the opening can start and continuous pumping of the fluid up the capillary channel can happen. Sometimes when the capillary force itself is not enough to pull the fluid up the channel, injection of fluid is needed to fill the channel of the capillary.
6. The fluid environment under the surface of human skin can be described as of negative pressure. It is unlikely the ISF will automatically fill the capillary by capillary effect. Even with the injection to fill the capillary beforehand, it still needs investigation that to see whether the pressure gradient established by atomization at the opening is enough to pull fluid up the capillary channel.

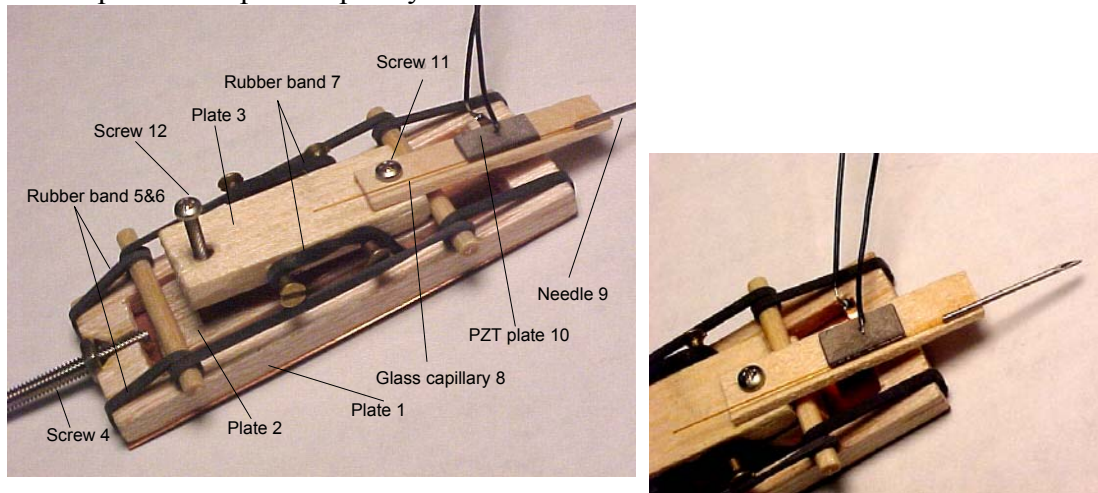


Figure G.2: Needle stage with elastic force feedback and ultrasonic capillary pump (23 gage stainless steel hypodermic needle, $200\mu\text{mOD}$, $100\mu\text{mID}$ glass capillary and $4\text{mm} \times 8\text{mm} \times 0.5\text{mm}$ PZT5 plate)

Projected efforts and anticipated results with quantitative measures if possible:

1. Collaboration with *Becton, Dickinson and Company* is in process to conduct in vivo animal experiments on needle insertion and ISF/blood sampling.

- Design and expand the system to include bioassay system and other components of the bioflip project. Figure G.3 shows one possible design that can be realized with plane springs made by plastic molding or lithography.

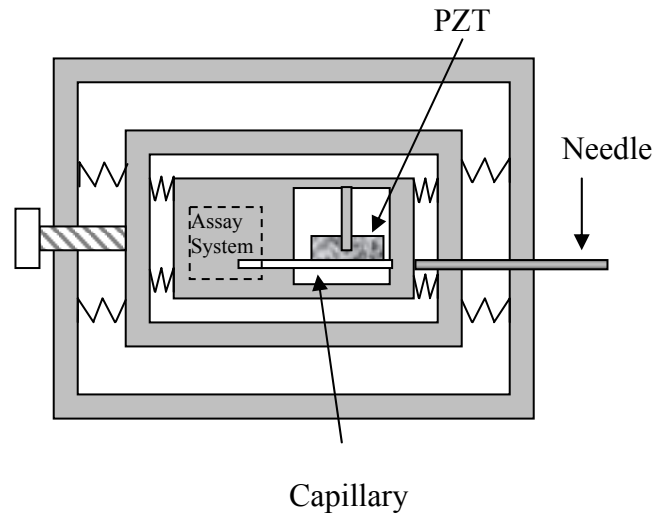


Figure G.3: A possible redesign of the needle insertion and pumping system

Description of needle stage and components as shown in Figure G.2

Solid plate 1 (5cm*2.5cm*0.3cm) is shaped into a rectangular frame. Solid plate 2 (4cm*1.5cm*0.3mm) is placed into this frame and can glide back and forth. Two rubber bands (5 and 6) are wrapped on the small extending parts on each longer side of plate 2 and then wrapped on plate 1, thus attach plate 2 to frame 1 but not fix the position of plate 2 relative to the frame. Screw 4 is put at the end of frame 1 and screwing in will push forward the plate 2 and therefore attached needle into skin, stretching rubber band 5 and 6 at the same time. Then screwing out 4 will release the rubber bands and the restoring force will pull the needle backward out of the skin.

Hypodermic needle 8 is glued and then fixed on solid plate 3 by screw 11. Plate 3 is attached to plate 2 through rubber band 7 in a similar manner as plate 2 is attached to plate 1. The rubber band on plate 3 provides the elastic feedback when the needle comes in contact with skin. When plate 2 moves forward to bring the needle tip into contact with skin surface, the resistance of skin causes rubber band 7 to be stretched backward. The restoring force of the rubber band increases as the resistive force of skin increases when the needle proceeds, and once the skin is penetrated there is usually a sudden release of the resistive force, and the rubber band 7 is released correspondingly and thus decreases the pushing force on the needle. Therefore, the needle would not keep proceeding after the skin is penetrated as in the case of constant force driven needle without feedback control. Screw 12 on plate 2 is used to adjust the angle of the needle against skin.

Section H:

Ultrasonic Separations and Pumping in Glass Capillary system

Chung-Hoon Lee (Ph.D. student) and Amit Lal

Goal: Beads can be coated with antibodies responsive to almost any antigen. Our aim in this research is to develop techniques to perform bead based assays using ultrasonics. In particular we use two acoustic fields to separate beads of different sizes in a capillary microfluidic system.

Documents available:

1. Lee, C., Lal, A., “Glass Capillary/PZT Transverse Wave Actuator for Microfluidic Radiation Force Assay,” IEEE Ultrasonics, Ferroelectrics, and Frequency Control Society Symposium, 2001, Atlanta
2. Lee, C., Lal, A., “Low-Voltage High-Speed Ultrasonic Chromatography For Microfluidic Assays,” Proceedings of the Solid State Sensor and Actuator Workshop, Hilton Head Island, South Carolina, 2002, pp. 206-209

Results:

Our previous reports indicate the work on using glass capillary and PZT system to pump – mechanism described in the needle project above. The pump project has led to ultrasonic separations that promise to hold great promise for fast-integrated bead-based assay on the Bioflip platform.

There is a need for separation of different size polystyrene beads coated with different antibodies for ratio in miniature biochemical systems. A typical electro-osmotic micro-fluidic assay system is shown in Figure H.1.

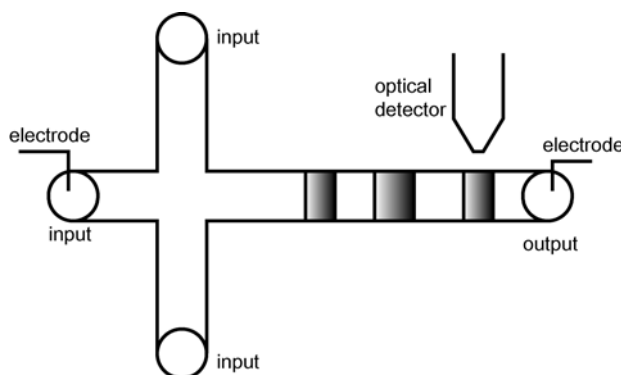


Figure H.1: A typical electro-osmotic micro-fluidic assay system.

Microfluidic devices utilizing differential mobility in a high electric field for beads/molecules require a conducting medium. However, uncertainty in medium conductivity requires accurate arrival time of particles to be detected at the fixed optical detection system.

The bead separation and particle manipulation with projected acoustic field has been investigated by many other workers. Acoustic radiation forces generated by concave transducer have been

used to concentrate particles at pressure nodes. Previous attempts for focusing beads at nodes using ultrasonic radiation force have led to increased detection limit of agglutination assays. However, separation of different sizes using the acoustic radiation force has not been demonstrated. The diffracted acoustic field from a particle leads to a non-symmetric acoustic field around the particle.

The nodes/antinodes in standing waves are usually sharp leading to beads clustering around a point and making separation of different size particles difficult. However, if one can widen the nodes/antinodes one can expect gradient of the radiation force acting on the mixed beads leading separation between different size beads at the broad nodes/antinodes. Furthermore the location of the beads are predictable and stable so that an optical detector can be placed to gather information for assays at the nodes/antinodes rather than across the entire glass loop (Figure H.2).

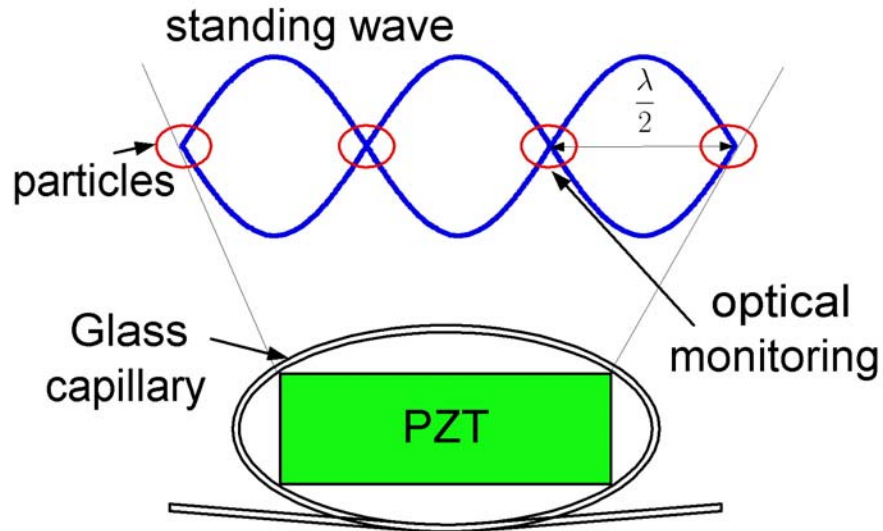


Figure H.2. Sketch of capillary bending mode.

2. Additional effects in glass capillaries

In addition to the effects of radiation pressure, the volume uptake of the particles in finite space of a glass capillary will lead to broadening of the bands formed by the beads. Since the force is proportional to the particle diameter cubed, one predicts that the large particles will move towards the antinodes with higher force leading to particle separation. Additionally, there is also a shear viscous acoustic field near the wall of the glass capillaries. This field causes acoustic streaming flow.

Beads in the acoustic field will move into nodes or antinodes depending on the sign of the acoustic contrast factor (F). If the F is positive, beads move toward the antinodes and if F is negative beads move toward the nodes. The density of polystyrene and speed of sound are 1.05 g/cm^3 and 2170 m/s , respectively, resulting in a positive sign of the acoustic contrast factor.

3. The Capillary/Glass Transducer

A schematic drawing of the glass capillary/PZT transducer is shown in Figure H.3. A polyimide coated glass capillary (ID = 100 μm , OD = 200 μm , polyimide thickness = 12 μm) is folded around the PZT plate (10 mm x 2.5 mm x 0.5 mm) with a knot. The knot acoustically decouples capillary modes from the inlet/outlet ends of the capillary so that any micro-fluidic boundary conditions can be applied to the system. For intimate contact, the glass capillary is adhesively bonded to edges of PZT plate using cyanoacrylate. A typical hand-assembled device is shown in Figure H.4. Two electrodes are soldered at the center of the PZT plate since a node of the displacement of PZT plate is at the center.

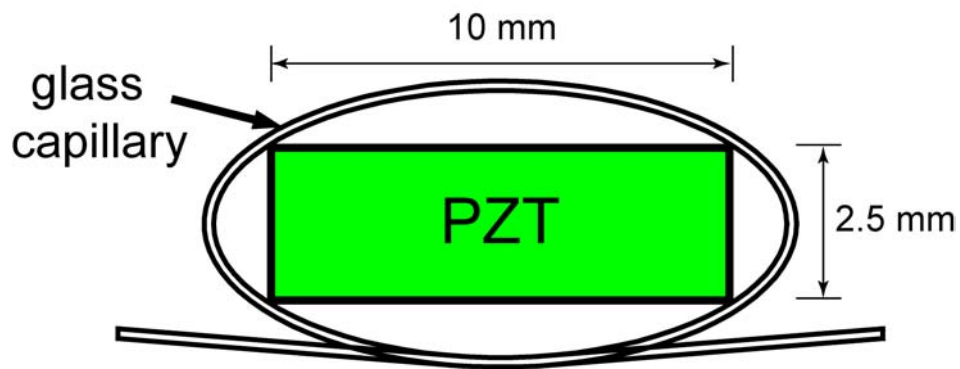


Figure H.3: A schematic drawing of the glass capillary/PZT transducer

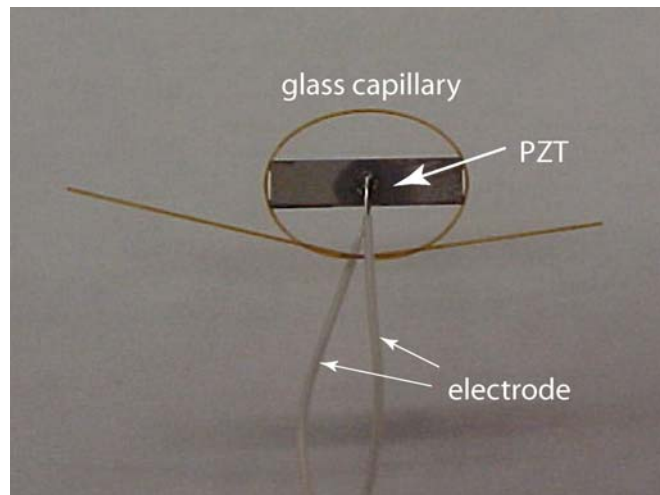


Figure H.4: The capillary/PZT transducer with electrodes.

There are two half-wavelength vibration modes of the PZT plate, namely the length mode and width mode (which is weakly coupled to bending modes) as shown Figure H.5.

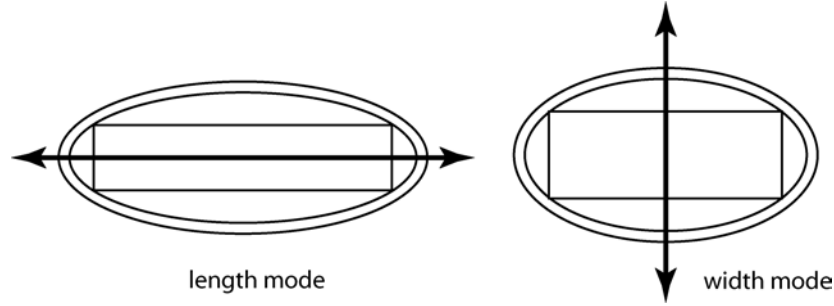


Figure H.5: Two half-wavelength vibration modes of the PZT plate.

Since these modes correspond to half-wavelength vibration, the two resonance frequencies are 160 kHz and 640 kHz respectively. Measured electrical impedance from HP4194 impedance analyzer is shown in Figure H.6.

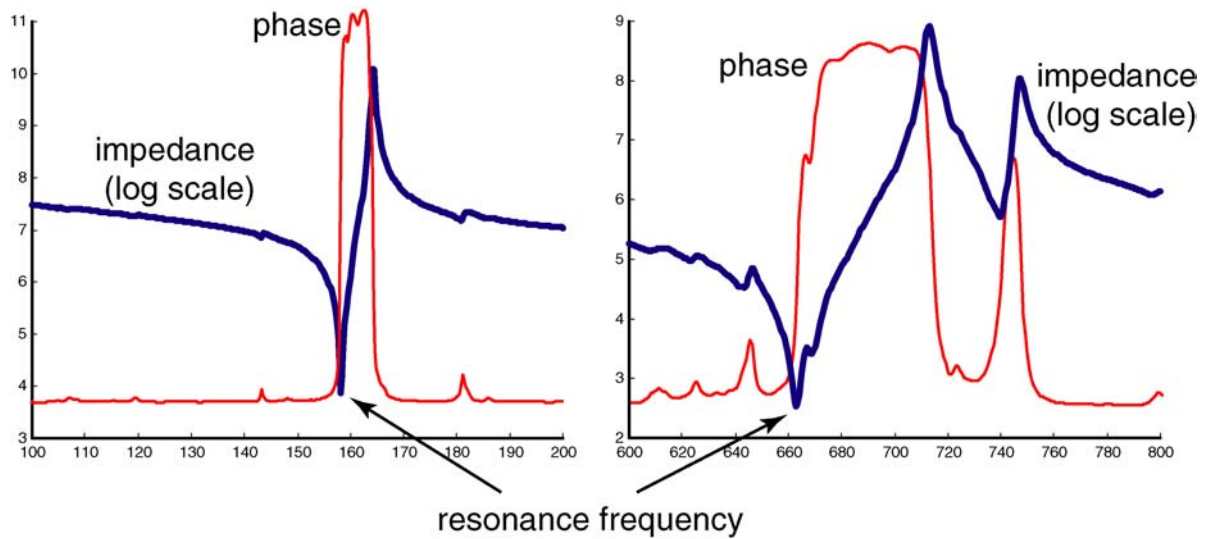


Figure H.6: Measured impedance of the PZT/glass transducer: left figure shows resonance frequency of the length mode (frequency: 160 kHz) and right shows resonance frequency of the width mode (frequency: 640 kHz).

4. Separation

A mixture of different size polystyrene beads was prepared for the separation experiment. As mentioned earlier, the polystyrene beads subjected in the acoustic field move into antinodes due to the density-compressibility factor regardless of size difference. However, the radiation force on the beads are proportional to the radius of the bead. Due to the different radiation force and gradient of the radiation force in the antinodes, beads that moved to antinodes were separated by size.

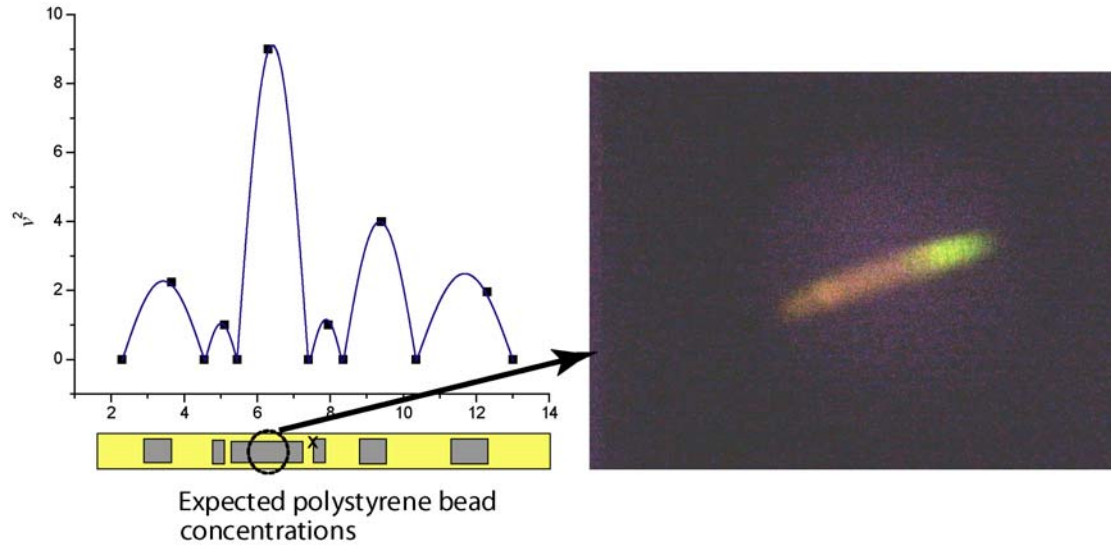


Figure H.7: Bead separation at a broad antinode: the size of the beads on left side is 1 μm and the size of the beads on right side is 5 μm .

Separation of beads at an antinode is shown in Figure H.7. The diameter of red fluorescence colored bead was 1 μm and that of green fluorescence colored beads was 5 μm . The driving voltage was 3 V_{pp} and the driving frequency was 160 KHz. As resonance frequency increases such as higher harmonics of the length modes or width modes, the broad band becomes sharp leading to difficulty in the separation process. Furthermore, the driving voltage has to be increased up to 7 V_{pp} for the effective separation.

Section I:

Brownian-motion Simulation of Particles in the Presence of Acoustic Radiation Forces

Jonathan D. Halverson (M.S. student), Michael Graham, Juan dePablo, and Amit Lal

Goals of project:

The overall goal of the project is to use computer simulation techniques to study the separation of mixtures of microparticles in the presence of an ultrasonic standing wave field.

A white blood cell count can be used to determine the health of a patient. If white blood cells could be extracted from a blood sample, optical detection methods could then be used to perform a count. One goal of this project is to use ultrasonic waves to create such a separation. Understanding the dynamics of binary systems will be the first priority. Special attention will be paid to the behavior of particles trapped by individual acoustic pressure nodes. We are also interested in knowing how acoustic intensity and particle size contrast influence separation.

A second goal of the project is to assess the feasibility of a new separation technique loosely termed acoustic chromatography. This is performed experimentally by first injecting the mixture into a microcapillary. Next, an ultrasonic standing wave is established in the axial direction. Finally, a motorized microliter syringe drives the fluid through the capillary. The acoustic force hinders the translation of the larger size particles more so than the smaller particles. This results in the smaller particles having a greater average velocity. Given sufficient time a separation will take place. Our model considers acoustic, viscous, excluded volume, and Brownian forces.

A separation technique is only useful to the lab-on-a-chip community if it can be performed over small length scales. The aim of our work here is to accomplish the same result as in the previously described acoustic chromatography but on a length scale of a few acoustic wavelengths. Two methods have been developed that meet this criterion. The first method requires choosing the acoustic parameters such that the larger particles are trapped at the first few acoustic pressure nodes. This method requires careful selection of the acoustic intensity, acoustic wavelength, and average fluid velocity. The second method involves adding a third component consisting of particles that are much larger in size than the largest size particle in the binary mixture. When introduced to the acoustic field these much larger particles migrate to the nearest pressure node where they arrange into an array. Particles whose diameter is less than some cutoff value may pass through the cavities in this array. Essentially, the third component organizes into a microscopic, semi-permeable mechanical filter. If this technique proves to work then separation will be possible on a length scale of less than an acoustic wavelength.

It is desired to simulate the motion of non-spherical particles undergoing acoustic chromatography. A goal of the project is to separate doublets or tangent-sphere dumbbells from single spherical particles. If such a separation were possible it would allow for the detection of nanomolar concentrations of proteins or macromolecules. This analytical technique is conducted by adding latex spheres, (coated with specialized antibodies), to the solution containing the antigen. Biomolecules containing two antigenic sites of differing type will each chemically bond

to corresponding antibody-coated spheres. After sufficient time has occurred for mixing, the solution consists of single spheres whose antibody coating has not reacted and doublets or complexes formed from two spheres whose antibody coating has reacted. Acoustic chromatography may then be used to separate the mixture. A count can be performed upon purification and (a) the presence of an antigen can be tested for or (b) the concentration of a particular antigen can be determined.

Previous results and status from last PI meeting:

At the last PI meeting our project was in its infancy. Below is an image of 1 and 2 μm particles after separation about a single acoustic pressure node:

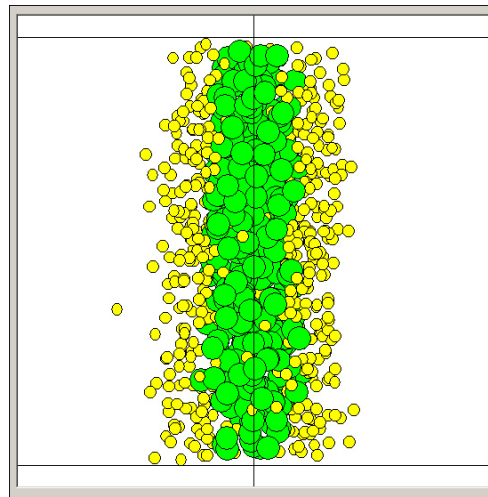


Figure I.1: Intranode Separation

We see that the larger particles, which experience the greater acoustic force, are positioned closest to the node. Due to excluded volume effects the smaller particles are displaced to the outside.

The idea of a microscopic mechanical filter was explored using particles of 30 μm in diameter. We attempted to separate a mixture of 1 and 5 μm diameter particles using the filter. Figure I.2 is a snap shot of the simulation:

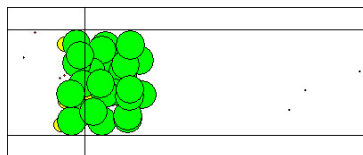


Figure I.2: Acoustic Filter

In the above figure, the direction of flow is from left to right. The large green particles are responsible for creating the filter. During the course of the separation their positions were

approximately constant. The image reveals that the $5\text{ }\mu\text{m}$ particles have been trapped by the array whereas the $1\text{ }\mu\text{m}$ particles have snaked through void pathways in the filter.

New results:

After enough data had been acquired, we began constructing mixing fraction diagrams for the intranode separation work. Mixing fraction is a measure of the overlap between layers or bands, which occur on either side of the pressure node. When the particle sizes are similar the mixing tends to be high. The figures below illustrate this trend for systems of 1 and $1.25\text{ }\mu\text{m}$ particles and 1 and $1.50\text{ }\mu\text{m}$ particles, respectively:

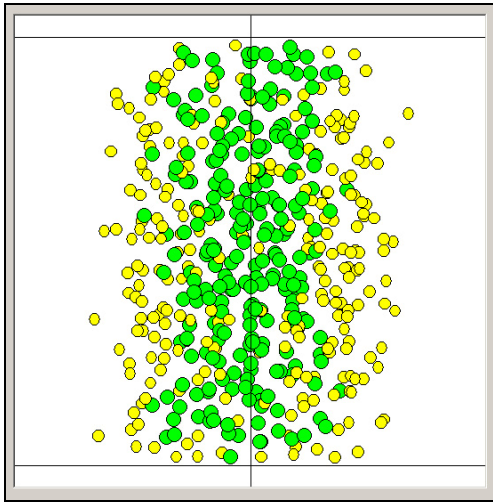


Figure I.3: 1/ $1.25\text{ }\mu\text{m}$

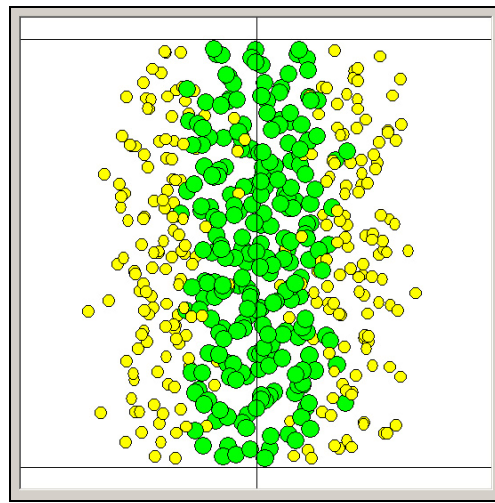


Figure I.4: 1/ $1.5\text{ }\mu\text{m}$

On comparison of Figures I.3 & I.4, band resolution is higher in Figure I.4 (where there is a greater difference in the size of the particles). It is important to know how the mixing fraction varies with particle size contrast. Figure I.5 is a mixing fraction plot for a base particle size of $1\text{ }\mu\text{m}$:

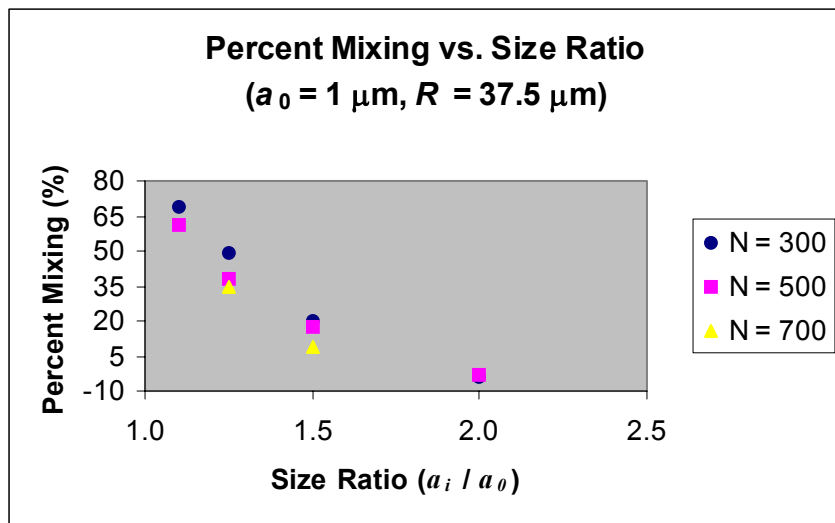


Figure I.5: Mixing Fraction Diagram

It is seen from Figure I.5 that as the size ratio approaches unity an appreciable separation does not take place. As the size ratio increases from unity the separation sharpens.

Through simulation we have been able to determine the required time to separate a mixture of particles in the continuous flow process (i.e., acoustic chromatography). We simulated the trajectories of particles flowing in a microcapillary subject to the effects of a standing wave established in the axial direction. We modeled a system where the wavelength was 1 mm, acoustic intensity of 0.1 W/cm^2 , average fluid velocity of 0.01 mm/s , and the radius of the capillary was $37.5 \mu\text{m}$. The 1200 particles of three different sizes were tracked for 89.5 hrs. in real time. The concentration and average position of the particles is shown below:

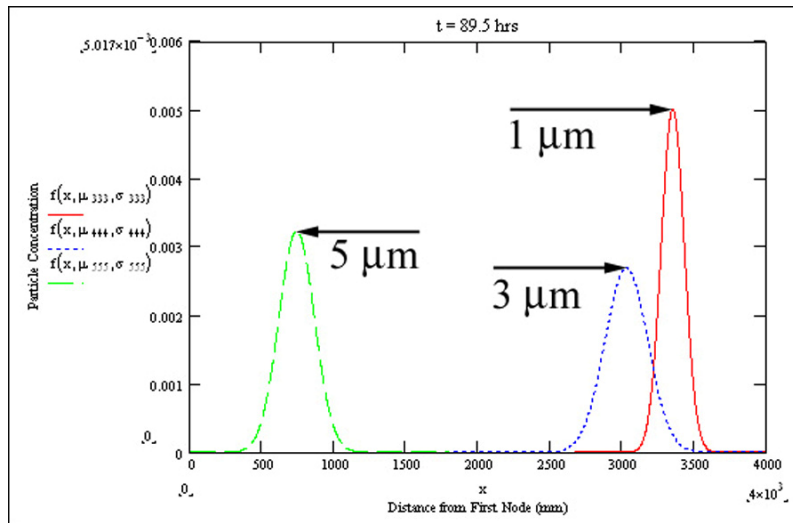


Figure I.6: Acoustic Chromatography

The results indicate that the 1 and 3 μm particles have completely separated from the 5 μm particles. Eventually the 1 μm particles will separate from the 3 μm particles yielding complete purification.

Next six month projected efforts and anticipated results with quantitative measures if possible:

Over the next six months we expect to distribute our efforts evenly over the four main areas of the project.

In our studies of intranode separations, we will be looking at the effect of acoustic intensity, wavelength, and particle size contrast on the degree of separation. It is expected that the degree of separation will sharpen as the acoustic intensity or difference in particle size increases. Data will be accumulated for various systems and plots clearly illustrating these trends will be constructed. We also intend to simulate these separations using an expression for the wave field of an experimental apparatus. We are interested in knowing how the results of computer simulation will compare to laboratory findings.

Section J:

Sensing protein conformational changes with resonant antennas

Kimberly Taylor (Ph.D. student) and Daniel van der Weide

Goals:

Determining changes in the conformation of proteins in solution is necessary for a variety of applications, including folding/unfolding thermodynamics and kinetics, enzyme catalysis and ligand binding. Water may be used as a reporter molecule for protein conformational changes. We propose the use of a resonant planar slot antenna to measure perturbations of the dielectric properties of water. Changes in permittivity within the near-zone of the antenna are reflected as shifts of the antenna's resonant frequency, which can be adjusted by changing the dimensions of the slot. Conformational change as determined by permittivity changes can be related and compared to conformational changes determined by other methods, such as UV/VIS or fluorescence spectroscopy.

Results:

We have designed, built, and tested a co-axial fed resonant slot antenna suitable for measuring changes in the conformation of proteins in solution. This antenna is fixed to the exterior of a fused quartz cuvette, allowing simultaneous microwave and UV/VIS spectroscopic measurements. Typical spectra obtained using these antennas are shown in Figure J.1.

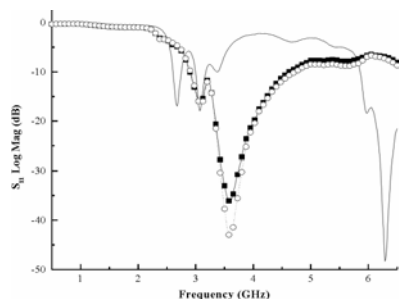


Figure J.1: Frequency response of air (solid line), buffer (■), and RNase A (○) as measured on an HP 8720D network analyzer

Changes in permittivity within the antenna's near zone, thought to be due to release or re-organization of water shells surrounding the protein, are reflected as shifts in the antenna's resonant peaks. The spectra in the frequency domain may be fitted to multiple Lorentzian peaks. Initial results indicate that the thermal response of these peaks yields sigmoidal curves typical of cooperative unfolding. Such a sigmoidal response was absent when a solution of buffer alone was heated under the same conditions.

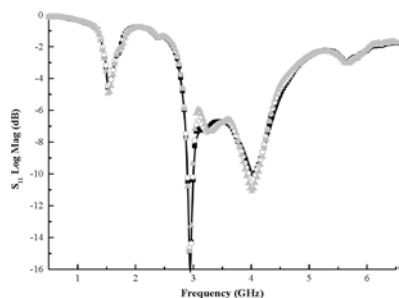


Figure J.2: frequency response of RNase A at selected temperatures. Symbols: 34.8 °C (solid line), 45.6 °C (■), 54.5 °C (○), 65.5 °C (▲)

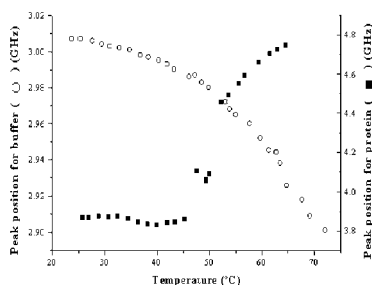


Figure J.3: Results of fitting of representative peaks from buffer (○) and protein solution (■). Note that protein peaks form a characteristic sigmoidal curve.

New results:

Bovine pancreatic ribonuclease A (RNase A), a small globular protein, was used for all experiments in a solution of 30 mM sodium acetate/acetic acid, 100 mM sodium chloride, pH 4.5. The positions of peaks in the microwave spectra were shown to vary approximately linearly with protein concentration.

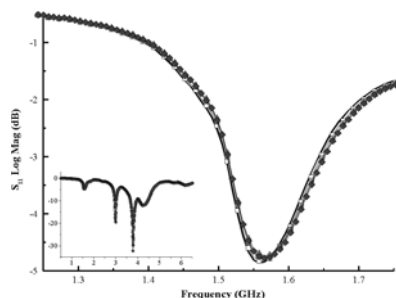


Figure J.4: Variation of peak position with concentration of RNase A. Inset shows complete spectra; close-up of a single peak is shown in the larger image. RNase A concentrations (mg/mL): 0 (solid line), 1.18 (□), 2.08 (●), 2.79 (◆), 3.35 (▲)

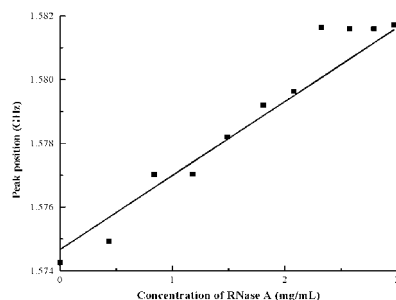


Figure J.5: Variation of peak 3 with RNase A concentration. Solid line indicates linear fit to data, with slope 2.75 MHz mg⁻¹ mL, intercept 1.57 GHz and R 0.984.

Thermal unfolding of RNase A was repeated multiple times, at concentrations varying from 0.2 to 1 mg/mL (14.6 to 73.0 μ M). Midpoint temperature (T_m , defined as the temperature at which 50% of the protein molecules are folded) and unfolding enthalpy (defined as the heat released upon unfolding 1 mole of protein) were invariant with protein concentration. After obtaining peak positions by fitting peak spectra to Lorentzian peaks, peak positions as a function of temperature were fitted to a two-state unfolding model. These curves yielded values of midpoint temperature (T_m) and unfolding enthalpy (ΔH_m) very similar to those results obtained from UV/VIS spectroscopy alone. These T_m and ΔH_m values also compare well to those obtained by other researchers. All experiments were performed at a low power range (-15 to +5 dB).

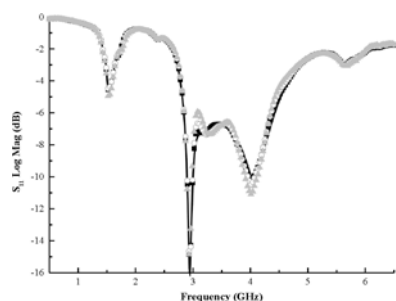


Figure J.6: frequency response of RNase A at selected temperatures. Symbols: 34.8 °C (solid line), 45.6° C (■), 54.5 °C (○), 65.5 °C (▲)

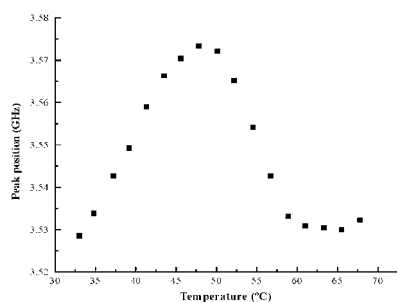


Figure J.7: variation of position of peak 5 with temperature.

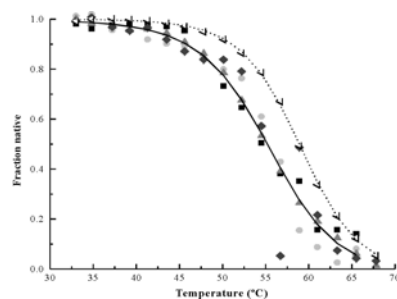


Figure J.8: Fits of data from microwave and UV/VIS measurements to 2-state unfolding model. Microwave data: peak 1 (■), peak 4 (●), peak 5 (▲), peak 7 (◆), fit to all peaks (solid line). UV/VIS data: data (◁), fit (dotted line).

	ΔH_m (kcal/mol)	T_m (°C)
Microwave (all peaks)	54.3	55.2
UV/VIS	61.3	59.2

Figure J.9 Results of fitting of data from microwave and UV/VIS measurements to 2-state unfolding model.

Next six month projected efforts and anticipated results with quantitative measures if possible:

Several important questions remain to be answered:

- 1) *Dependence of unfolding results on microwave power*: Although initial results indicate that the protein is not destabilized by the presence of microwave radiation, additional experiments are needed. Unfolding at a single protein concentration will be repeated at a variety of power settings. It is expected that midpoint temperature T_m and unfolding enthalpy ΔH_m will not depend on microwave power.
- 2) *Effect of microwaves on enzyme activity*: RNase A is an enzyme that cleaves single-stranded RNA in solution. This reaction can be monitored using UV/VIS spectroscopy. Two questions can be answered here. First, can the activity of RNase A and/or the cleavage of RNA be detected using our antenna system? Second, does microwave power have any effect on the rate or efficiency of cleavage?
- 3) *Detection of protein-ligand association*: Using a non-hydrolysable RNA analog, we will attempt to detect the binding of RNA to RNase A. In addition, the binding of ribonuclease inhibitor (RI) to RNase A can also be detected. RI binds tightly to RNase A and inhibits its enzymatic functions.
- 4) *Other proteins and/or biological molecules*: Our system can be extended to the study of other proteins and other biological systems (hybridization of DNA/RNA, melting of lipids, etc.).

Appendix 1 List of Publications

1. Lee, C., Lal, A., "Low-Voltage High-Speed Ultrasonic Chromatography For Microfluidic Assays," Proceedings of the Solid State Sensor and Actuator Workshop, Hilton Head Island, South Carolina, 2002, pp. 206-209
2. Radhakrishnan, S., Solak, H., Lal, A., "In-channel flow sensor using drag forces," Proceedings of the μ TAS 2001 Conference, Monterey, CA, pp. 179-181, Kluwer
3. Sathaye, A., Lal, A., "An acoustic vortex particle concentrator," Proceedings of the μ TAS 2001 Conference, Monterey, CA, pp. 185-187, Kluwer
4. Lee, C., Dong, Y., Lal, A., "A glass-PZT Ultrasonic Microfluidics Platform," Proceedings of the μ TAS 2001 Conference, Monterey, CA, pp. 489-491, Kluwer
5. Siwaponrsathain, E., Lal, A., "Micromachined Ultrasonic Si/PZT Transducer for Underwater Communications," IEEE Ultrasonics, Ferroelectrics, and Frequency Control Society Symposium, 2001, Atlanta
6. Hang, G., Lal, A., "Flexural plate wave excitation using bulk modes," IEEE Ultrasonics, Ferroelectrics, and Frequency Control Society Symposium, 2001, Atlanta
7. Hang, G., Lal, A., "Characterization of Silicon Nitride Membranes Using Resonant Ultrasound Spectroscopy," IEEE Ultrasonics, Ferroelectrics, and Frequency Control Society Symposium, 2001, Atlanta
8. Kaajakari, V., Lal, A., "Optimization of a Bulk-Driven Surface Micromachined Ultrasonic Micromotor," IEEE Ultrasonics, Ferroelectrics, and Frequency Control Society Symposium, 2001, Atlanta
9. Lee, C., Lal, A., "Glass Capillary/PZT Transverse Wave Actuator for Microfluidic Radiation Force Assay," IEEE Ultrasonics, Ferroelectrics, and Frequency Control Society Symposium, 2001, Atlanta
10. Sathaye, A., Lal, A., "An acoustic vortex generator for microfluidic particle entrapment," IEEE Ultrasonics, Ferroelectrics, and Frequency Control Society Symposium, 2001, Atlanta
11. Ochoco, J., Lal, A., "Programmable Acoustic Streaming on a 2D PZT Pixel Array," IEEE Ultrasonics, Ferroelectrics, and Frequency Control Society Symposium, 2001, Atlanta
12. Ochoco, J., Lal, A., "Resonance Frequency Tuning of Two-Dimensional PZT array using Laser Trimming," IEEE Ultrasonics, Ferroelectrics, and Frequency Control Society Symposium, 2001, Atlanta
13. Chen, X., Lal, A., "Integrated Pressure and Flow Sensor in Silicon-Based Ultrasonic Surgical Actuator," IEEE Ultrasonics, Ferroelectrics, and Frequency Control Society Symposium, 2001, Atlanta
14. Chen, Xi, Lal, A., "Micromachined Ultrasonic Ophthalmic Microsurgical tool with integrated Pressure sensor," Digest of Technical Papers, International Conference on Solid State Sensors and Actuators, Munich, pp. 424-427
15. Kaajakari, V., Sathaye, A., Lal, A., "A Frequency Addressable Ultrasonic Microfluidic Actuator Array," Digest of Technical Papers, International Conference on Solid State Sensors and Actuators, Munich, pp. 958-961
16. Masters thesis: Jomar Ochoco, 2002, UW-Madison
17. Masters thesis: Abhijit Sathaye, 2002, UW-Madison
18. Masters thesis: Jon Havelson, 2002, UW-Madison
19. Undergraduate Research Report: Enny Kho, 2002, UW-Madison
20. PhD Thesis: Ville Kaajakari, 2002, UW-Madison

Appendix 2 PATENTS: Disclosures/Filings with WARF (Wisconsin Alumni Research Foundation)

Filed patents

1. Beam flow sensor
2. Integrated pressure sensor on needle structure
3. Vortex particle collector
4. Ultrasonic Chromatography

Disclosures

1. 2D PZT pixel array and electronics
2. Magnetic pillar formation
3. Microfluidic valve with magnetic pillar with piezoelectric actuation
4. Ultrasonic separations in glass capillary structures
5. Needle insertion jig with elastic feedback

Appendix 2 Student Contributions

- Chung-Hoon Lee – Separations and glass/capillary/PZT structures –ECE – Graduating with PhD in August 2002 – Will continue as postdoc
- Xi Chen – Microneedle work –ECE – Ph.D. student – will continue at Cornell
- Jomar Ochoco – PZT arrays – ECE – Graduated with M.S. in summer 2002
- Shankar Radhakrishnan – Flow sensing –ECE – Ph.D. student – will continue at Cornell
- Rajesh Duggirala – PZT micromachining – microvalves – ECE – M.S. student, will continue at Cornell
- Il-Seok Son – Piezoresistive sensors and magnetic extrusion – ECE – Ph.D. student, will continue at Cornell
- Enny Kho – Sine wave generation – Undergraduate –ECE - Graduated
- Abhijit Sathaye – Vortex particle collector – ECE – M.S. student - graduated
- Jon Haverlson – Ultrasonic separation modeling – Chemical Engineering – M.S. student - graduated
- Kimberly Taylor – RF detection of proteins- Biotechnology – Ph.D. student, graduated